

THE FLORIDA STATE UNIVERSITY
COLLEGE OF ARTS AND SCIENCES

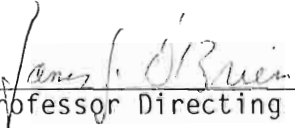
OBJECTIVE ANALYSIS ALGORITHM FOR
SATELLITE SURFACE WIND DATA

by

DAVID M. LEGLER

A thesis submitted to the
Department of Meteorology
in partial fulfillment of the
requirements for the degree of
Master of Science

Approved:



Professor Directing Thesis





April, 1984

April, 1984

ABSTRACT

A technique is developed to derive surface synoptic wind fields from fields sampled by a space-borne scatterometer. The data are generated using a three-dimensional (latitude, longitude, time) interpolation scheme applied to the 1000-mb FGGE data set in the north Pacific. These sampled data simulate the sampling of future scatterometer missions. Two-day average maps were calculated using the simulated data and then compared to the original two-day average of the FGGE data.

The first case used data containing no added error. In the second case, random white noise was added to the sampled wind vectors to simulate errors inherent in scatterometer sampled data. In the final case, spatially correlated noise was added to the sampled swaths to reflect possible errors due to sampling winds with both synoptic and mesoscale components.

The resultant two-day average maps were good representations of the original maps. The average magnitudes of the difference vectors, original minus analyzed, were never more than about 2.75 ms^{-1} . These values were considerably less than the spatial average of the temporal variability of the original two-day average maps. Adding random noise to the sampled fields did not have much effect of the temporal variability of the original two-day average maps. Adding random noise to the sampled fields did not have much effect

on the resultant maps. Adding the spatially correlated noise increased the errors more than random noise of the same magnitude. The binning and filtering processes reduced the effects of the added errors noise.

The results signify the dependence on the sampling characteristics of the scatterometer, rather than on instrument noise or spatially correlated noise of substantial magnitude.

ACKNOWLEDGMENTS

I would like to personally express my gratitude to Dr. J. J. O'Brien for his support and guidance during the past years. Our discussions have been enlightening. Thanks for believing in me. Thanks also to Drs. J. Stephens and S. Stage for serving on my thesis committee and offering insight and assistance to my research. To all the members of the Mesoscale Air-Sea Interaction Group, I express my heartfelt thanks for the wonderful assistance and encouragement. A special thanks to Helen McKelder who cheerfully typed the numerous versions of this thesis. Thanks finally to my wife Nan for her love and understanding throughout the last year.

This research was supported by the National Aeronautics and Space Administration under contracts NAG5-219 and NGT-10-004-800 at Florida State University. Computations were performed on a CDC Cyber 170-760. I am grateful to Dr. J. Marsh of NASA-Goddard for providing the satellite ephemeris data.

A special appreciation to my grandmother Margaret, who first awakened my love for meteorology: may she be pleased with my efforts.

TABLE OF CONTENTS

	Page
ABSTRACT	ii
ACKNOWLEDGMENTS	iv
TABLE OF CONTENTS	v
LIST OF TABLES	vi
LIST OF FIGURES	vii
INTRODUCTION	1
GENERATION OF THE DATA SET	6
METHOD	
ANALYSIS OF DATA WITH NO ADDED NOISE	12
ANALYSIS OF DATA WITH ADDED UNCORRELATED NOISE	38
ANALYSIS OF DATA WITH ADDED SPATIALLY CORRELATED NOISE	42
DISCUSSION OF RESULTS	57
SUMMARY AND CONCLUSIONS	60
REFERENCES	63

LIST OF TABLES

TABLE		PAGE
1	Table of wavenumber filter cutoffs and the resultant spatial average of the difference field between the original vectors and the vectors resulting from filtering with the cutoff values for the first example in the no-noise case. Units are ms^{-1} .	22
2	Numerical characteristics of the method and the results for the two examples in the no-noise case.	27
3	Numerical characteristics of the method and the results for examples in the case with spatially correlated noise added to the swaths.	50

LIST OF FIGURES

FIGURE		PAGE
1	Configuration of NROSS satellite.	7
2	Area of interest for this study: 145°E to 135°W, 30°N to 50°N.	8
3	Orbital and ground track characteristics of the simulated satellite used to sample the data. The 500 km swaths are perpendicular to the ground track. In this idealized case, swath width is constant. Note there are no observations immediately below the satellite.	10
4	Two-day average for the first example in the no-noise case: January 10-11, 1979. Units on this and all vector plots are ms^{-1} .	13
5	Data sampled by the imaginary satellite during Jan. 10-11 averaged into 50-km cells. Darkened vectors indicate interpolation was used to calculate the vector.	15
6	Enlargement of the eastern portion of the basin in Fig. 5. Every other vector is plotted for easier analysis. Darkened circles at any location indicate interpolation was used to calculate the vector analysis. Darkened circles at any location indicate interpolation was used to calculate the vector	16

7	The 100-km cell data from binning the 50-km cell data for the first example in the no-noise case.	17
8	Wavenumber response function for the filter. The wavenumbers are relative to the cutoff wavenumber. Large scale waves are to the left, small scale waves to the right.	20
9	The 100-km data representing the two-day average as a result of a low-pass filter with wavenumber cutoffs of 5 in longitude and 3 in latitude for the first example in the no-noise case.	23
10	Vector difference, $\vec{V}_{\text{Original}} - \vec{V}_{\text{Analyzed}}$, of the 100-km filtered data for the first example in the no-noise case.	24
11	Two-day average for the second example in the no-noise case: January 20-21, 1979.	30
12	Data sampled by the imaginary satellite during Jan. 20-21 averaged into 50-km cells. Darkened vectors indicate interpolation was used to calculate the vector.	31
13	Enlargement of the eastern portion of the basin in Fig. 12 . Every other vector is plotted for easier analysis. Darkened circles at any location indicate interpolation was used to calculate the vector. indicate interpolation was used to calculate the vector.	32

14	The 100-km cell data from binning the 50-km cell data for the second example in the no-noise case.	33
15	The 100-km data representing the two-day average as a result of a low-pass filter with wavenumber cutoffs of 4 in longitude and 11 in latitude for the second example in the no-noise case.	34
16	Vector difference, $\vec{V}_{\text{Original}} - \vec{V}_{\text{Analyzed}}$, of the 100-km filtered data for the second example in the no-noise case.	35
17	Data sampled by the imaginary satellite during Jan. 20-21 in the eastern half of the basin averaged onto a 50 km grid. Uncorrelated white noise of standard deviation 2 ms^{-1} was added to each observation. Every other vector is drawn for easier analysis. Darkened circles indicate interpolation was used to calculate the vector.	40
18	The 100-km cell data from binning the 50-km cell data of Fig. 17.	41
19	Data sampled by the imaginary satellite during January 20-21 in the eastern half of the basin with spatially correlated noise with a standard deviation of 2 ms^{-1} added to each swath. Every other vector is drawn for easier analysis. Darkened circles indicate interpolation was used to calculate the vector drawn for easier analysis. Darkened circles indicate interpolation was used to calculate the vector	45

20	The 100-km cell data from binning the 50-km cell data with spatially correlated noise of standard deviation 2 ms^{-1} added to each swath.	46
21	The 100-km data representing the two-day average as a result of a low-pass filter with wavenumber cutoffs of 4 in longitude and 11 in latitude applied to the data in Fig. 20.	48
22	Vector difference, $\vec{V}_{\text{Original}} - \vec{V}_{\text{Analyzed}}$, of the 100-km filtered data of Fig. 21.	49
23	Data sampled by the imaginary satellite during January 20-21 in the eastern half of the basin averaged onto a 50 km grid. Spatially correlated noise with a standard deviation of 3 ms^{-1} is added to each swath. Every other vector is drawn for easier analysis. Darkened circles indicate interpolation was used to calculate the vector.	52
24	The 100-km cell data from binning the 50-km cell data of Fig. 23.	53
25	The 100-km data representing the two-day average as a result of a low-pass filter with wavenumber cutoffs of 4 in longitude and 8 in latitude applied to the data in Fig. 24.	54

26 Vector difference, $\vec{V}_{\text{Original}} - \vec{V}_{\text{Analyzed}}$, of the 100-km filtered data of Fig. 25. 55

INTRODUCTION

Since the first meteorological satellite was placed into orbit in 1960, meteorologists have continually strived to improve the methods of observing and remotely sensing all the common meteorological variables. The microwave scatterometer is an instrument for remotely measuring the surface winds over the ocean.

After much development and testing, the idea of a space-borne scatterometer became a reality in 1978 with the launching of SEASAT. During its three months of operation, a unique data set was obtained, and SEASAT demonstrated the scatterometer could perform well. (Jones *et al.*, 1982, Liu and Large, 1982, and Brown, 1983; for an excellent review of the development of the scatterometer, and details of how it derives wind vectors, see O'Brien *et al.*, 1982) There were, however, three primary problems with the SEASAT scatterometer data.

The first problem was probably the most obvious; because of the design of the scatterometer, the measured wind vector could have as many as four directional solutions or ambiguities (sometimes called aliases). This necessitated a monumental task of de-aliasing the observations into the proper directions. Some schemes have been developed to accomplish this task (Wurtele *et al.*, 1982).

developed to accomplish this task (Wurtele *et al.*, 1982).

A second problem encountered in the SEASAT scatterometer data were the effects of communication noise errors, satellite attitude errors, and errors resulting from using an empirical model to derive the wind vectors as functions of the sensed backscatter. In addition, corrections for liquid water in the atmosphere reduced the accuracy of the scatterometer. The impact of these errors on future scatterometer missions will be lessened because of the extensive analysis of the SEASAT data in an attempt to improve the instrument.

The third problem in the data set is the problem considered presently. The asynoptic sampling scheme of the scatterometer on a polar-orbiting satellite is very unique. The problem occurs primarily because weather systems move quickly across the earth. The satellite will sample an area, and upon sampling the area again, the storm system will have moved to another location. Thus, the newly sampled data does not correspond to the same weather system. A simple method of assimilating the data onto a regular grid for a synoptic map is not straightforward.

Meteorologists have extensive experience in interpreting synoptic maps on a rectangular grid and little experience in using data from a polar orbiting satellite in its original space-time scheme. This paper tests various objective analysis procedures to obtain synoptic maps from asynoptic data. These should be useful for atmospheric and oceanic modelling.

for atmospheric and oceanic modelling.

Several researchers have studied the sampling of polar orbiting satellites. Chapman and McGregor (1978) used complex demodulation to analyze Nimbus radiometer data. This method did not provide any information in the high frequency end of the spectrum since a 3-4 day smoothing was applied. Hayashi (1980) presented a method to estimate space-time spectra of data from polar orbiters. Salby (1982a, b) has developed an extension of the Sampling Theorem to allow a Fast Fourier Transform Scheme to retrieve the unique sequence of synoptic maps from the satellites' asynoptic data. The allowed region of the spectra is analagous to that of "twice-daily" synoptic sampling at equidistant points numbering close to the orbital frequency (about 14). This allowable region could theoretically be extended, since in his paper, Salby assumed one observation per satellite "look," whereas for the scatterometer, each "look" provides up to 20 data points.

This present paper will examine the sampling problem of the scatterometer and develop an analysis technique to find synoptic maps of two-day averages from the asynoptically sampled data. The ease of using this analysis method will make it beneficial for operational use.

A known gridded data set, FGGE level III-b, is sampled by a simulated polar-orbiting satellite with instrument design features similar to future scatterometer missions. The analysis technique similar to future scatterometer missions. The analysis technique

utilizes spatial and temporal averaging and Fourier wave-space filtering to produce refined representations of the two-day average on a rectangular grid using only the remotely sensed data. The generated maps are compared to the original two-day averages. The two-day period was chosen for two reasons. It is usually the minimum time necessary to have at least one observation on all but about 5% of a region. More than 95% coverage would take a much longer time. The second reason for choosing the two-day period is the result of typical time scales for weather system passages in the area of this study. This time scale is usually 2-8 days. Since it is advantageous to find an average map for the shortest period possible, the two-day period was chosen.

Several simulations are analyzed in this paper. First, an optimal data set is constructed from the data sampled by the scatterometer aboard an imaginary satellite. This data set contains no errors because it is derived from the original wind fields. An objective analysis method is developed to estimate this two-day average map of the basin, using only the sampled data. In the second case, uncorrelated white noise is added to each observation to simulate the inherent errors of real scatterometer data. Lastly, the third case is an analysis of data that have spatially correlated noise added to each swath to reflect a sampling of a field which

results in data with both synoptic and mesoscale components in it. All of the three cases use the same basic analysis method, but fine tuning is used in an attempt to obtain optimal results.

GENERATION OF THE DATA SET

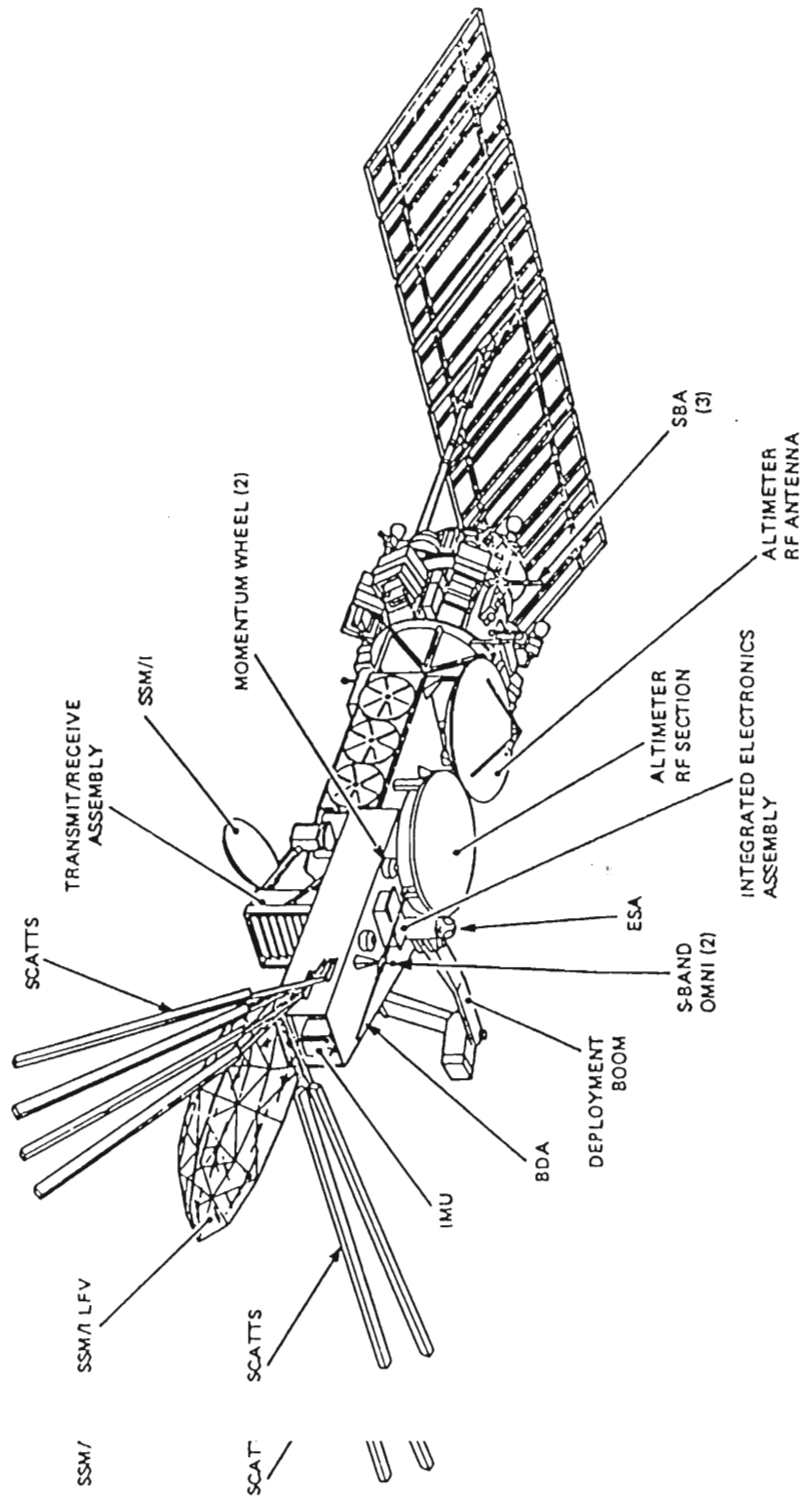
Because of the previously discussed problems with the SEASAT data, a useable de-aliased data set has not yet become available. Therefore, a data set was created to simulate the sampling of the N-ROSS (Navy Remote Ocean Sensing System) scatterometer which will be in orbit in late 1988, Fig. 1. The sub-satellite track of an imaginary polar-orbiting satellite was provided by J. Marsh, NASA, Goddard Space Flight Center. The simulated satellite was placed in an orbit similar to that of the future satellite and sampled the FGGE data set.

This data set was extracted from the FGGE level III-b data set (Bengtsson *et al.*, 1982). These winds are on a 1.875° degree grid at numerous pressure levels, and are computed every 12 hours. During the special observing periods (winter and summer months), the winds are available every 6 hours. For the time period of interest, the data were available every 6 hours.

For this study, the winds on the 1000 mb surface were extracted for the area 145°E to 135°W , and 30°N to 50°N which covers the North Pacific Ocean south of the Aleutian Islands, Fig. 2.

This area was chosen because of the consistent passage of synoptic scale winter storm fronts through the area every of 2-8 days. Choosing an area of non-varying winds would prove pointless synoptic scale winter storm fronts through the area every of 2-8 days. Choosing an area of non-varying winds would prove pointless

NROSS Configuration



RAE Astro-Electronics

Fig. 1. Configuration of NROSS satellite.

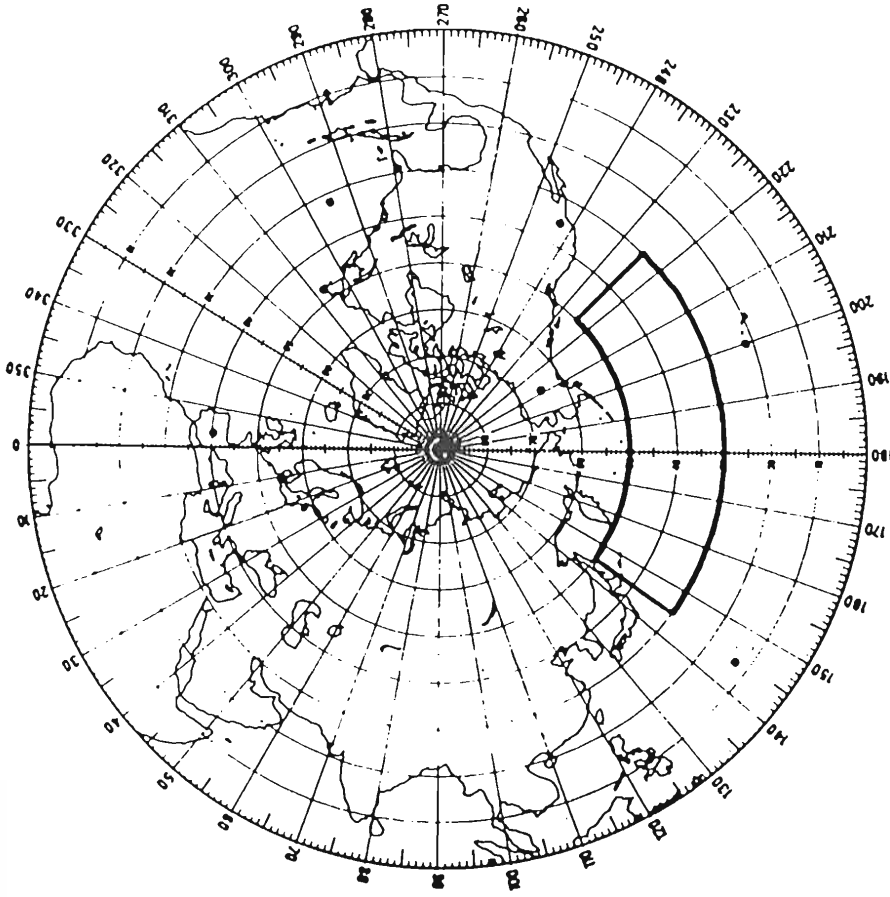


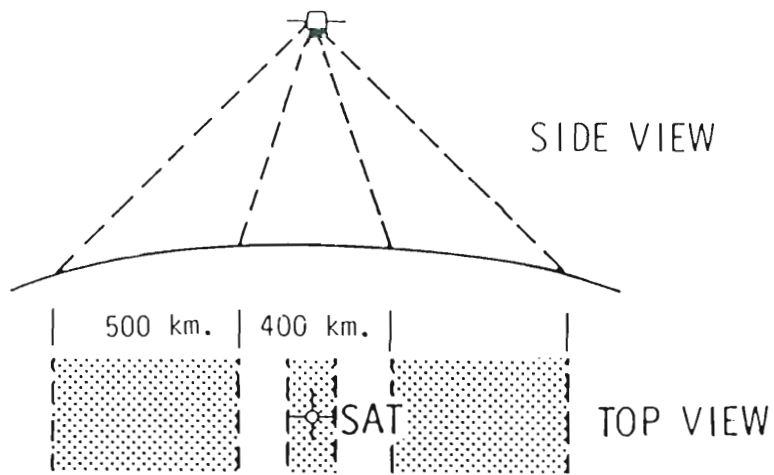
Fig. 2. Area of interest for this study: 145°E to 135°W, 30°N to 50°N.

since one sampling would then provide all the information wanted irrespective of the satellite orbital frequency. The continually changing weather pattern is important in testing the synoptic analyses of the region. This area is an area of strong developing winter storms.

Figure 3 gives the orbital description of the satellite and the idealized ground coverage of the imaginary satellite. The satellite asynoptic data set consists of wind vectors every 50 km perpendicular to the ground track and every 50 km along the ground track. The vectors were computed by using a three-dimensional (x,y,t) linear interpolating scheme applied to the FGGE data set. The locations of each sampling by the scatterometer are known. The interpolation scheme provides wind vectors at all of these sampling locations.

Does this simulated sampling of model resultant winds properly reflect true scatterometer sampling? The model used to produce the FGGE level III-b winds used real winds as input. Of course, the model's smoothing schemes may be subject to examination, but the resultant data set is representative and is a synoptic field.

However, a true scatterometer samples a field containing both a synoptic and a mesoscale component. Pierson (1983) and Pierson and Salfi (1982) discuss some aspects of remotely sampling these fields. Using Monte Carlo techniques, they find the mesoscale contribution
Using Monte Carlo techniques, they find the mesoscale contribution



Orbital Period	101 minutes
Orbital Frequency	$14.25 \text{ rev day}^{-1}$
Inclination Angle	98.7°
Altitude	833 km.

Fig. 3. Orbital and ground track characteristics of the simulated satellite used to sample the data. The 500 km swaths are perpendicular to the ground track. In this idealized case, swath width is constant. Note there are no observations immediately below the satellite

to the signal masked by communication noise variability in the 10 km cells sensed by N-ROSS. These cells are binned to produce the 50-km cell observation. Pierson finds the noise variability masks the mesoscale contribution in the 50-km cell, but not as severely as in the finer resolution cells. Pierson's results indicate mesoscale variability is very difficult to resolve in real scatterometer sampling. The generated data is similar to sampling an almost pure synoptic field. Later in this paper, generated spatially correlated noise will be added to the swaths sampled by the scatterometer to simulate the effects of mesoscale winds on the analysis.

METHOD

ANALYSIS OF DATA WITH NO ADDED NOISE

The first case will have as its input the "perfect" original data set. The imaginary satellite will sample the FGGE data set as it is. The data sampled by the scatterometer will not be contaminated with communication noise, there will be no missing values, and the direction of the winds are known. This is an optimal case, and the results are expected to be optimal.

Beginning January 10, 1979 at 00 GMT, 8 map times (available every 6 hours) were averaged into the two-day average map for Jan. 10-Jan. 11, Fig. 4. This is the wind field which the objective analysis technique will try to reproduce using the scatterometer winds. The average wind speed in this field is $.8.4 \text{ ms}^{-1}$ and the variance of the wind speed is $12.7 \text{ m}^2\text{s}^{-2}$. The variance of this field can be expressed by the vector variance

$$\overline{\sigma_v^2} = \frac{1}{NM} \sum_{xy} |\vec{v} - \bar{\vec{v}}|^2$$

where N and M are the number of points in longitude and latitude respectively. In addition, $\bar{\vec{v}}$ is the average vector wind of the field. This vector variance has a value of $62.8 \text{ m}^2 \text{ s}^{-2}$ for this field. This vector variance has a value of $62.8 \text{ m}^2 \text{ s}^{-2}$ for this

10
→

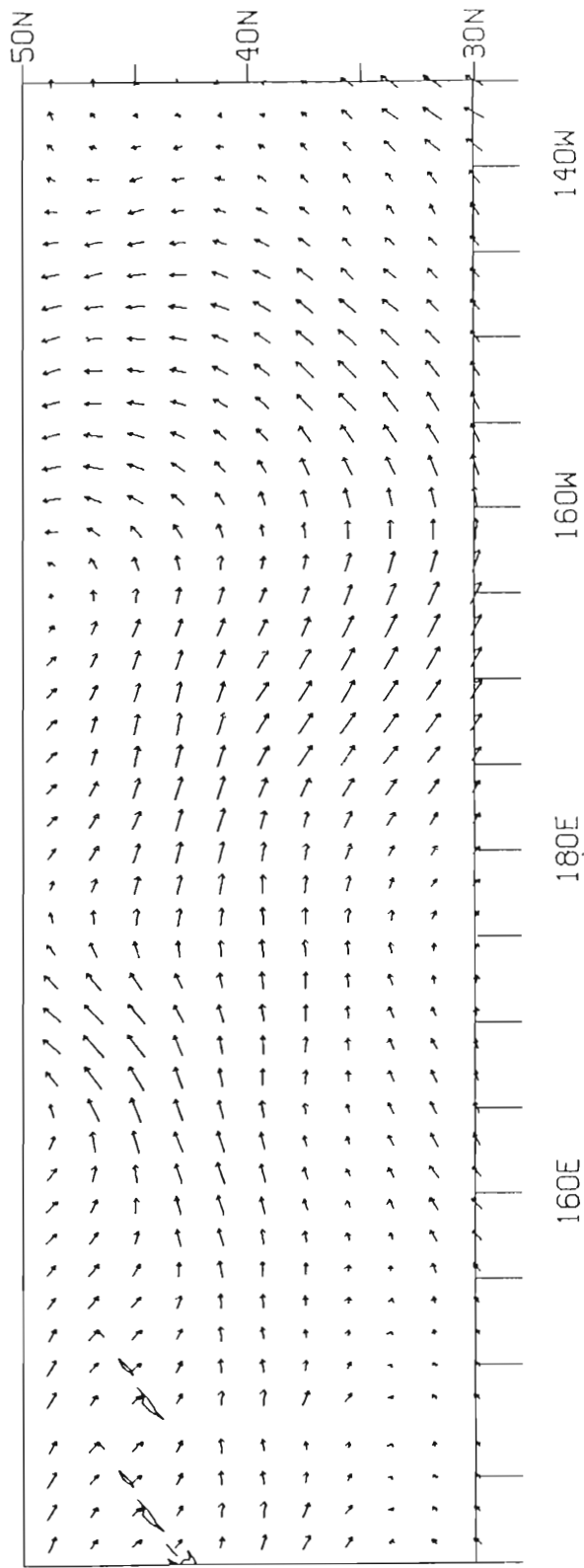


Fig. 4. Two-day average for the first example in the no-noise case: January 10-11, 1979. Units on this and all vector plots are ms^{-1} .

first case. In addition, the standard deviations of the wind speeds temporal records at each point were averaged spatially. This number, 4.65 ms^{-1} for this first case expresses an overall view of the wind speed variability in the basin. Both of these numbers will be used later when comparing the original map to the objectively analyzed map. The wavenumber spectra of this average field is red, indicating little small scale spatial variability.

To simulate scatterometer sampling, the satellite was flown through the FGGE data set beginning at 00 GMT, Jan. 10. After 49.2 hours, the satellite completed 17 passes over the basin. This time length was chosen to insure at least a two-day sampling period and an integral number of passes through the data.

The satellite sampled data were averaged onto a 50-km grid, Figs. 5 and 6. Data void regions created by placing this grid on the raw averaged data were filled by east-west linear interpolation. The triangular shaped data void regions in the southern portion of the basin are characteristic of polar-orbiter sampling and were also filled by linear interpolation.

The data were binned into 100-km boxes to reduce the size of the data set, Fig. 7. This binning has the effect of smoothing the spectra. In addition, this binning increases the number of scatterometer observations available at each point to calculate the

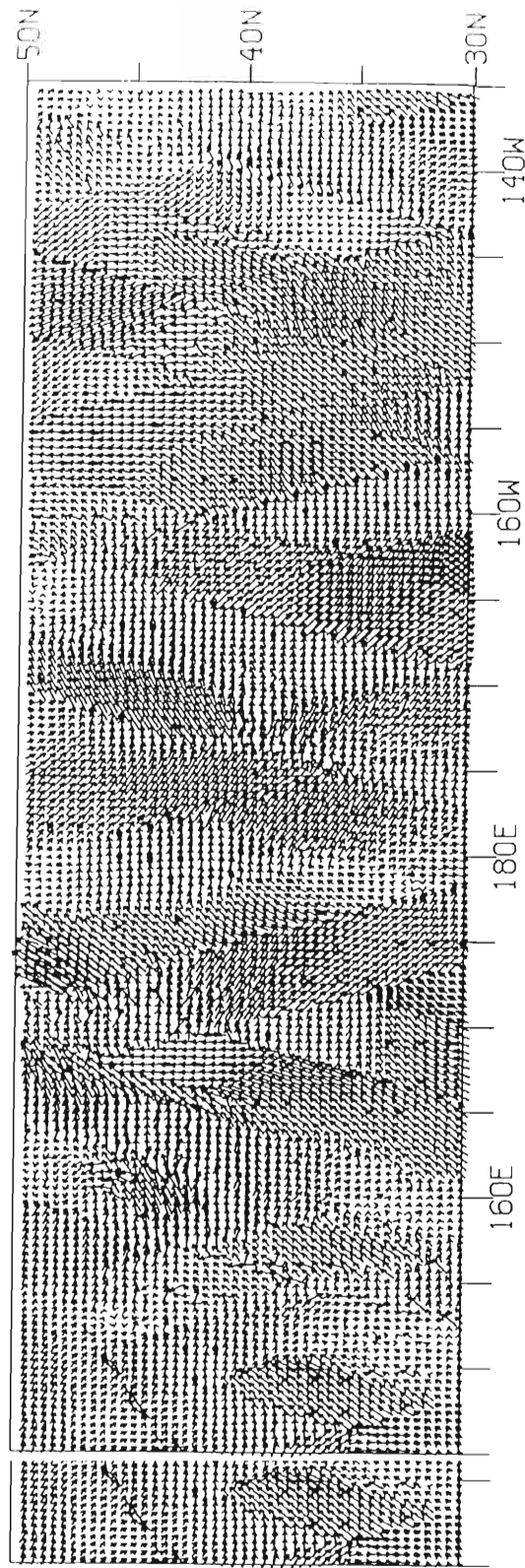


Fig. 5. Data sampled by the imaginary satellite during Jan. 10-11 averaged into 50-km cells. Darkened vectors indicate interpolation was used to calculate the vector.

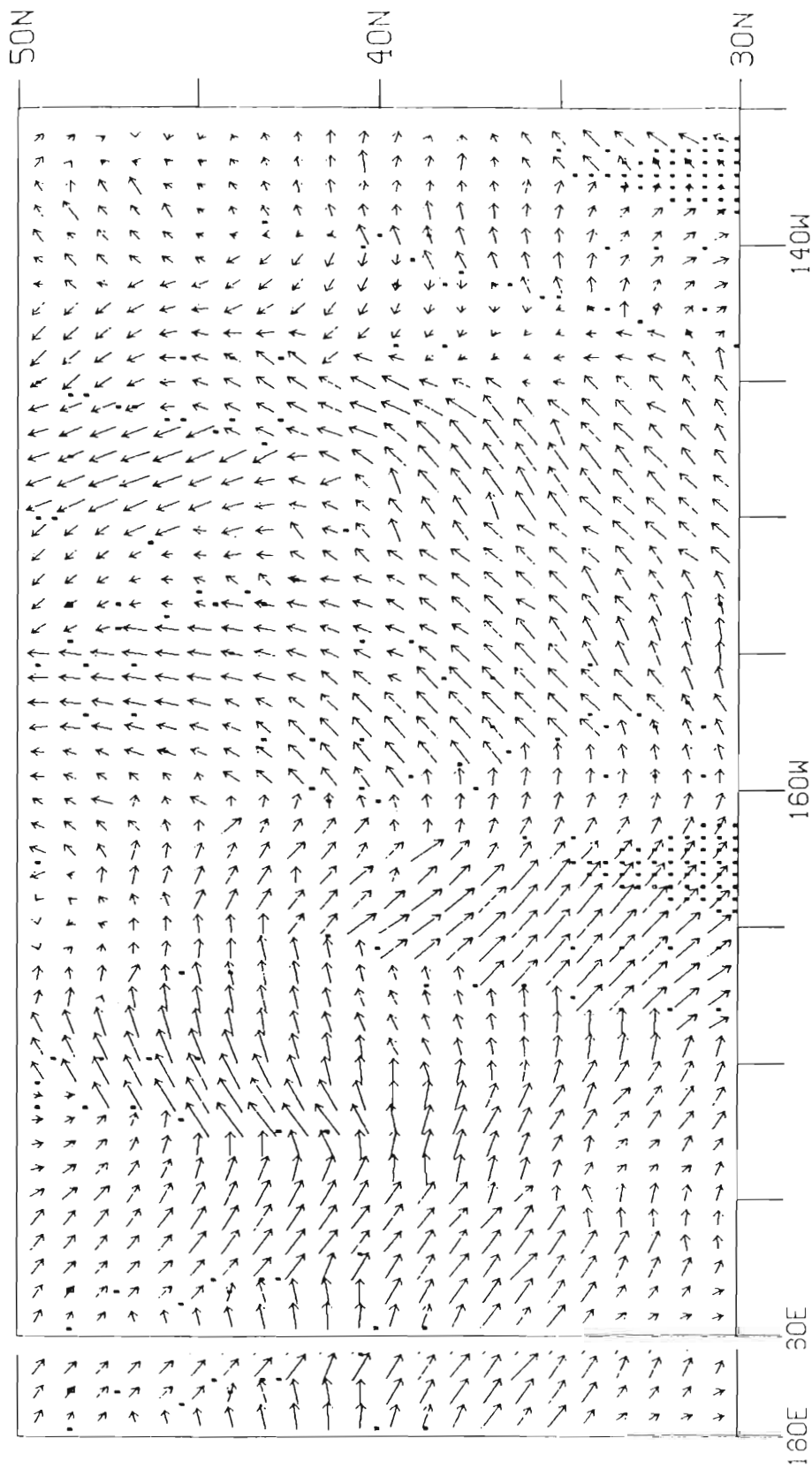


Fig. 6. Enlargement of the eastern portion of the basin in Fig. 5. Every other vector is plotted for easier analysis. Darkened circles at any location indicate interpolation was used to calculate the vector.

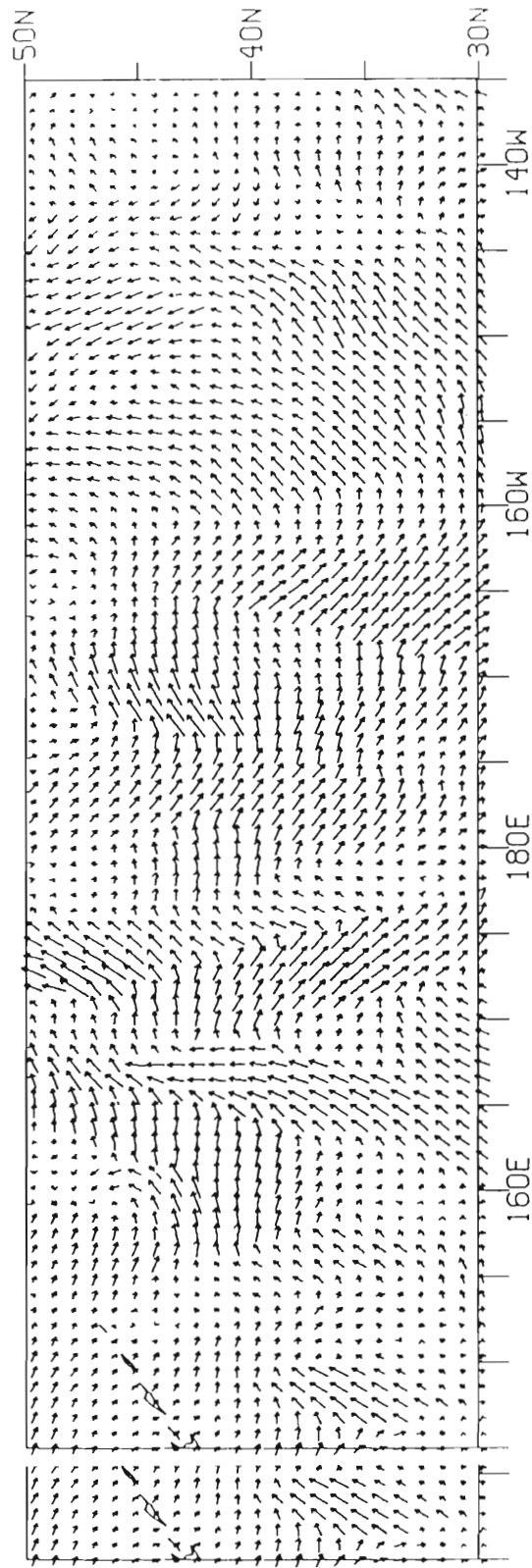


Fig. 7. The 100-km cell data from binning the 50 km cell data for the first example in the no-noise case.

average map for this two-day period. The swath paths are still evident in this data; they appear as wave-like patterns of wavelength more than 600 km, about 5° in longitude. In particular, note the unevenness of the magnitudes in the longitudinal direction. As the result of satellite sampling, these regions of strong winds then weak winds, possibly in another direction, then strong winds again or perhaps in reversed roles, will be the areas of error when the final objectively analyzed map is compared to the original two-day average map.

The scatterometer sampled data has aliased extraneous and obviously incorrect signals into a wide range of wavenumber components. The range of contaminated components is difficult to determine and not well understood since the wind spectra over the ocean is not well known particularly over the mid-latitude regions. (See Gallegos-Garcia, *et al.*, 1980 for recent work). In this 100-km gridded data, and the 50-km gridded data, extraneous contributions to the data occur primarily in the longitudinal, x-direction, as a result of the sampling instrument moving discontinuously in the longitudinal direction. In the latitudinal, y-direction, the sampling is relatively continuous during the 100-minute swaths through the data, but very asynoptic when several swaths of data are overlaid onto the 50-km and then the 100-km data fields.

Both the 50-km and the 100-km gridded data have red spectra

Both the 50-km and the 100-km gridded data have red spectra

with some energy evident at shorter wavelengths. Since the original two-day average has a very red spectrum, the next step is to apply a low-pass filter to the 100-km gridded data. The filter was applied in wavenumber space to insure no data loss at the boundaries, as is the case when using spatial filters. The filter should not filter out important spectral components provided the filter characteristics and cutoff values are carefully chosen. A filter with a sharp cutoff would dictate that a critical choice needs to be made concerning the cutoff values. Using a smoother filter, the decision is not as delicate. Thus the filter design chosen does not have a sharp cutoff, Fig. 8. The design of the filter was chosen by testing many different designs to test for optimal results. The sharpness as well as the wavenumber span were varied to find the design resulting in the best results. Cutoff is defined here as being the first wavenumber with a weight less than 0.5. This design was chosen as a result of many empirical tests using a test data field. Extensive tuning and improvement of the filter is certainly a topic of additional research.

Since the data are two-dimensional, a cutoff wavenumber was chosen in latitude and longitude wavenumber space. The final choice for these two values was determined in the same way as the filter design. The data were filtered with various cutoff values, and the cutoffs resulting in the best representation of the original two-day average were selected. The conclusions section will discuss cutoffs resulting in the best representation of the original two-day average were selected. The conclusions section will discuss

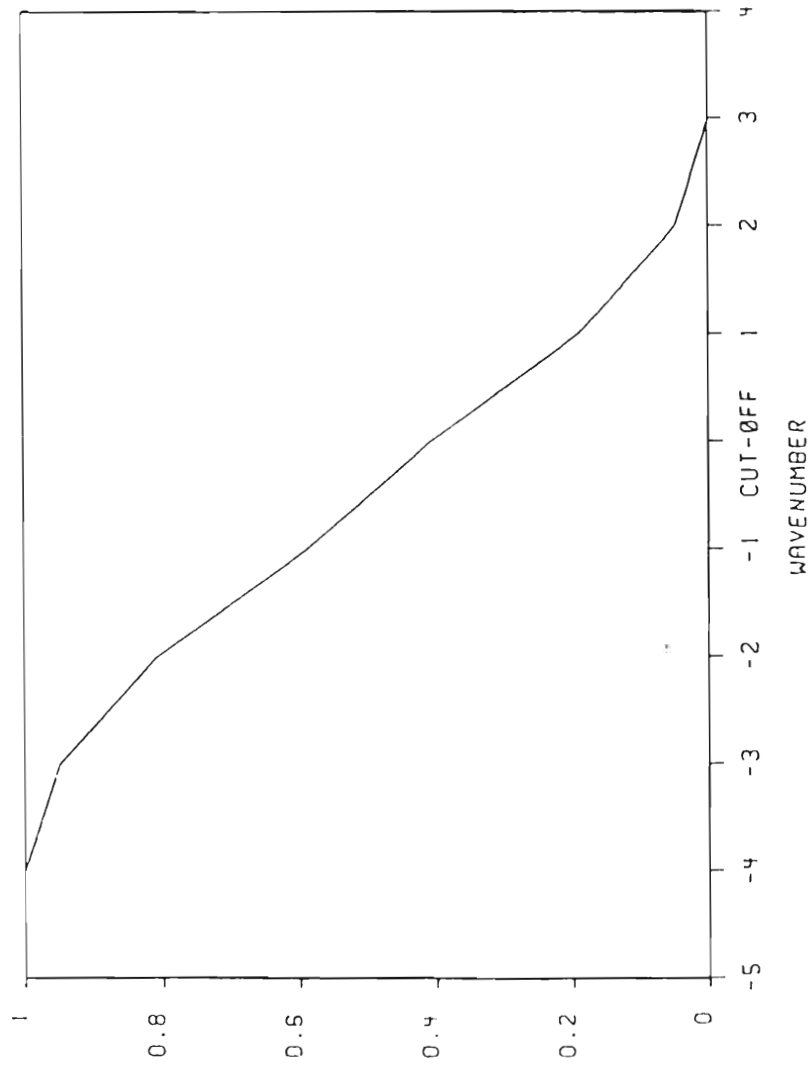


Fig. 8. Wavenumber response function for the filter. The wavenumbers are relative to the cutoff wavenumber. Large scale waves are to the left, small scale waves to the right.

suggestions for cutoff values in the future when the original two-day average is not known. As previously mentioned, the majority of the extraneous spectral components will probably appear in the longitudinal wavenumber space rather than the latitudinal wavenumber space. Table 1 demonstrates how changing cutoff values affects the mean magnitude of the difference vectors original minus analyzed. The cutoff values of optimal benefit are wavenumber 5 in the x-domain, and wavenumber 3 in the y-domain, Fig. 9. [Wavenumbers in this context refer to wavenumbers in the area of interest. Thus a wavenumber 1 in the latitudinal direction would have a wavelength of 20° or about 2200-km]. The cutoff values in latitude and longitude filter scales smaller than 800-km and 1800-km, respectively. The differences between the errors for wavenumber cutoffs 3, 5, 7, 9, and 11 in latitude, for a cutoff value of 5 in longitude are not very large. The cutoffs can be varied slightly without major consequences. In the next example, the best combination is 4 in x and 11 in y, thus allowing almost all of the latitudinal spectral components to remain in the data.

The vector variance of this field, Fig. 9, is $29.4 \text{ m}^2\text{s}^{-2}$. The vector variance compares fairly well to the vector variance of the original two-day average field. This objectively analyzed map is smoother than the original map.

The vector difference, original minus objectively analyzed maps, is shown in Fig. 10. The comparison of the original two-day
The vector difference, original minus objectively analyzed maps, is shown in Fig. 10. The comparison of the original two-day

Table 1. Table of wavenumber filter cut-offs and the resultant spatial average of the difference field between the true vectors and the vectors resulting from filtering with the cut-off values. This is for the first example in case 1. Units are ms^{-1} .

		x direction cut-off			
		3	5	7	9
y direction cut-off	3	3.15	2.66	3.07	3.09
	5	2.99	2.76	3.31	4.05
	7	2.95	2.73	3.31	4.05
	9	2.93	2.71	3.30	4.04
	11	2.92	2.69	3.28	4.04

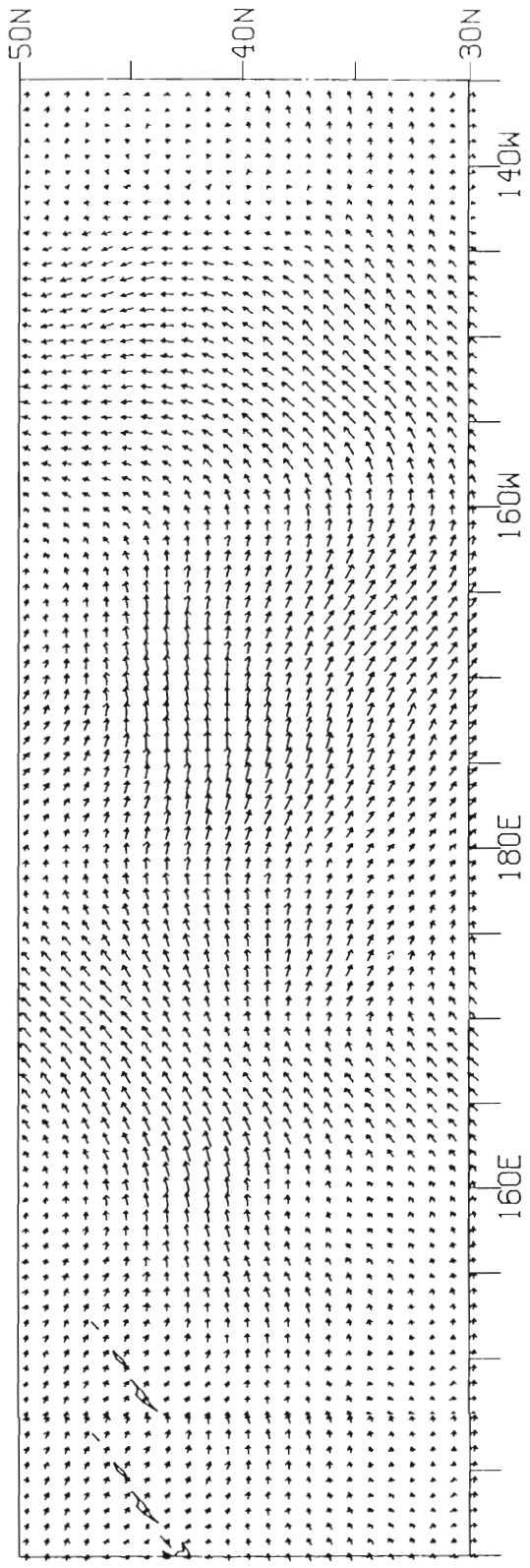


Fig. 9. The 100-km data representing the two-day average as a result of a low-pass filter with wavenumber cutoffs of 5 in longitude and 3 in latitude for the first example in the no-noise case.

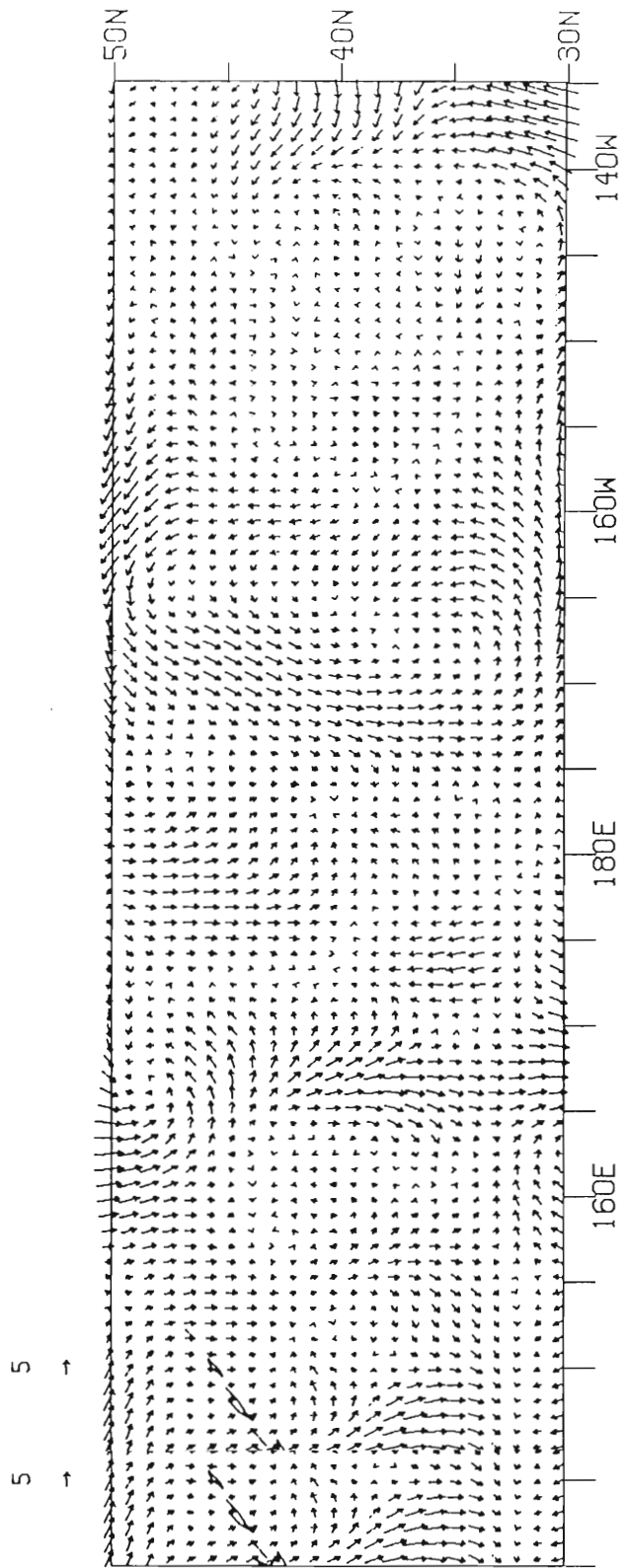


Fig. 10. Vector difference, $V_{\text{original}} - V_{\text{analyzed}}$, of the 100-km filtered data for the first example in the no-noise case.

average data to the objectively analyzed data required that the original data be linearly interpolated to the points on the objective analysis' 100-km grid. This interpolation comparison method was chosen to focus on the 100-km grid; comparison data on the larger grid would not reflect a test of the finer resolution. There is however, a spectral modification because of the interpolation. Overall, the resultant map faithfully reproduces the gross features of the original data, but fails to identify some variations in these features. For example, the analysis did not pick up the full intensity of the cyclonic structure in the northwest quadrant of the basin. Some features did not appear because of the sampling. For instance, at 30°N , 140°W to 135°W , the true data shows southwesterlies. But even in the 50-km data, the winds are northwesterly thus almost nullifying any chances for a correct representation in this area. The small area of southwesterlies along the eastern border may have helped bring about westerlies instead of the desired south-westerlies.

The resultant map is a striking result when considering that most of the locations on the 50-km grid are the result of at most 3 observations (samplings) by the satellite. The process of binning these observations into the 100-km boxes combines 4 of these observation collections to produce a map which will then be filtered. But in this binning process, the locations are close filtered. But in this binning process, the locations are close

together spatially and usually temporally. In summary, most of the vectors in the analyzed map have been synthesized from a collection of four spatial observations, each sampled at nearly the same time. Each of these four observations is the result of at most 2 or 3 separate sampled vectors, measured at different times by the scatterometer. In fact the analysis method does an excellent job of reproducing a map which used 8 distinct observations in time at each point.

There are several important structures to note in Fig. 10. The areas of highest error occur where the sampled data are "discontinuous" in x . This is easiest to see in the area between 165°E and 175°E and between 30°N and 40°N . In the 100-km data, looking from west to east there are south-westerlies then westerlies and then north-westerlies. By examination, such a pattern is abnormal. This type of problem is evident throughout the basin.

A numerical comparison can be made between the two maps, Table 2. The vector difference is the best estimate of the error between two vector fields. The average magnitude of the difference vectors is 2.67 ms^{-1} . This error is smaller than the spatial average of the temporal standard deviations of the true map, 4.65 ms^{-1} . Thus the errors are significantly smaller than the temporal variability of the original data, an indication that the method provides an excellent result. The spatial average difference between the true magnitude and the objective analysis' magnitude is very near 0 for excellent result. The spatial average difference between the true magnitude and the objective analysis' magnitude is very near 0 for

Table 2. Numerical characteristics of the method and the results for the two examples in the no-noise case.

	example 1: Jan 10-11	example 2: Jan 20-21
Spatial average of temporal std. dev. ms^{-1} .	4.65	4.68
Vector variance of the FGGE two-day average field m^2s^{-2} .	62.8	71.79
Optimal wave-number filter cutoff: longitude, latitude.	5,3	4,11
Vector variance of the objectively analyzed field m^2s^{-2} .	29.4	56.3
Spatial average of difference vector magnitudes ms^{-1} .	2.66	2.64
Spatial average of difference vector u components ms^{-1} .	1.53	1.43
Spatial average of difference vector v components ms^{-1} .	1.83	1.94
Vector variance of difference field m^2s^{-2} .	9.55	9.58

this and all the examples in this paper. In addition, the average difference in direction between the true data and the analysis is less than 5° in all the cases.

For comparison, Whitney (1983) compared cloud wind vectors and rawinsonde derived wind measurements from several international programs. He found the RMS vector difference, satellite cloud vector-rawinsonde vector, to be greater than about 7 ms^{-1} using low clouds in determining the cloud wind vectors. Thus, cloud wind vectors do not provide good estimates of winds over the ocean, even if the rawinsonde winds were accurate. Other methods of calculating winds over the ocean such as buoys or ships may be more accurate, but none have the spatial resolution of the scatterometer or even have a 100-km resolution.

The vector variance of the error field for this first example is $9.55 \text{ m}^2\text{s}^{-2}$. The vector variance of the error is much less than the vector variance of the original field. The analysis has produced a good approximation to the true data field since the error variance is much less than the vector variance of the true field, and the average magnitude of the difference vectors is significantly smaller than the temporal variability. In comparison, without filtering, the average magnitude of the difference vectors is 5.3 ms^{-1} . Filtering, therefore, has improved the analysis. Binning the data into 100-km observations also aided in lowering the error. If data into 100-km observations also aided in lowering the error. IT

the data remained on the 50-km grid, the mean magnitude of the difference vectors is over 8 ms^{-1} regardless of filtering characteristics. This is the obvious result of not having enough observations at each point to reproduce faithfully the average map.

A second example was calculated using the optimal data set. The data begins January 20, 1979 at 00 GMT. The original two-day average, Fig. 11, has an average wind speed of 8.52 ms^{-1} and a wind speed variance of $19.7 \text{ m}^2\text{s}^{-2}$. The vector variance is $71.79 \text{ m}^2\text{s}^{-2}$ and the spatial average of the standard deviations of wind speed is 4.68 ms^{-1} .

The same process is applied to this second example as before. The data sampled by the scatterometer were gridded into 50-km boxes, Figs. 12 and 13, and then binned onto a 100-km grid, Fig. 14. The optimal filter was similar to that chosen in the first example. The cutoff values in this case were wavenumber 4 in longitude and wavenumber 11 in latitude. This resultant field is shown in Fig. 15. The vector variance of this resultant map is $56.3 \text{ m}^2\text{s}^{-2}$; close to that of the original data field.

In this example, the numerical comparison was about the same as the previous example. The average magnitude of the difference vectors is 2.64 ms^{-1} . The vector variance of the difference field is $9.58 \text{ m}^2\text{s}^{-2}$. The difference field, Fig. 16, demonstrates how the error is distributed in patches. The largest area of error is error is distributed in patches. The largest area of error is

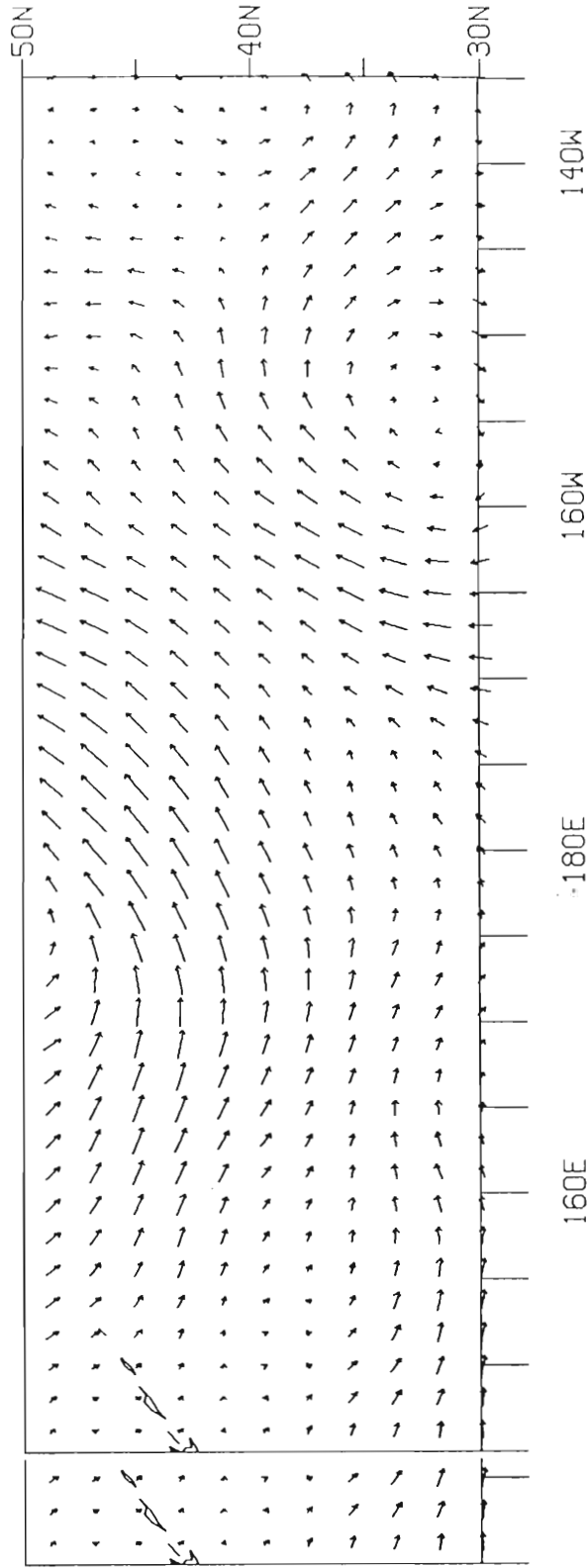


Fig. 11. Two-day average for the second example in the no-noise case: January 20-21, 1979.

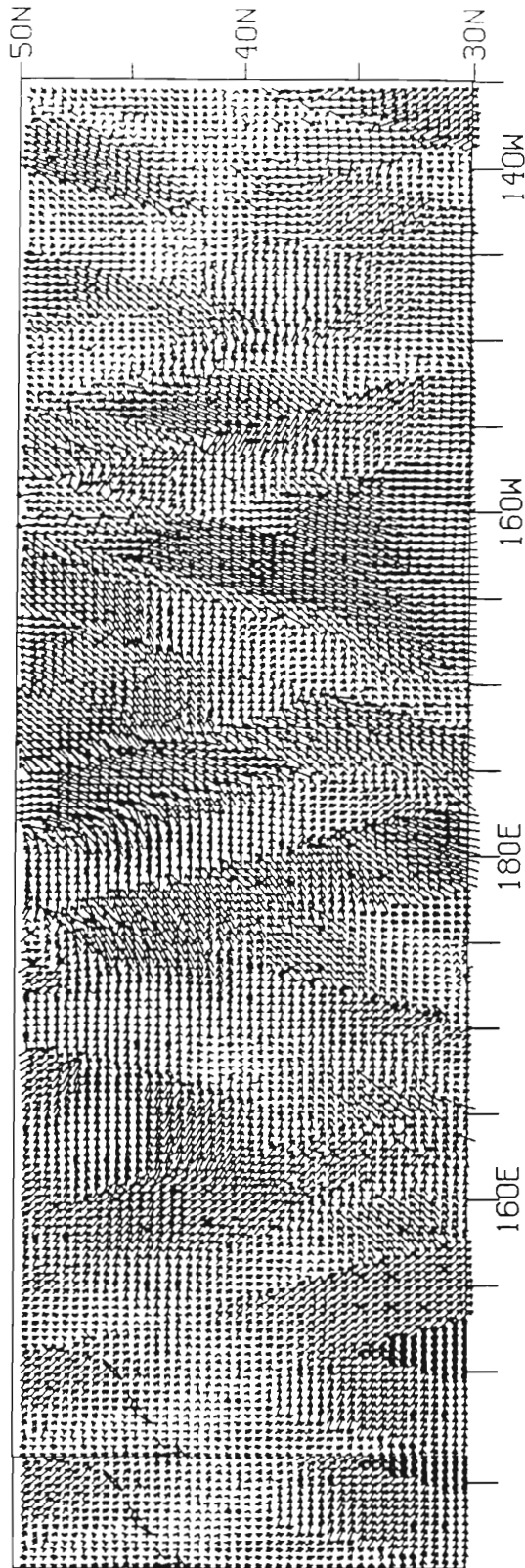


Fig. 12. Data sampled by the imaginary satellite during Jan. 20-21 averaged into 50-km cells. Darkened vectors indicate interpolation was used to calculate the vector.

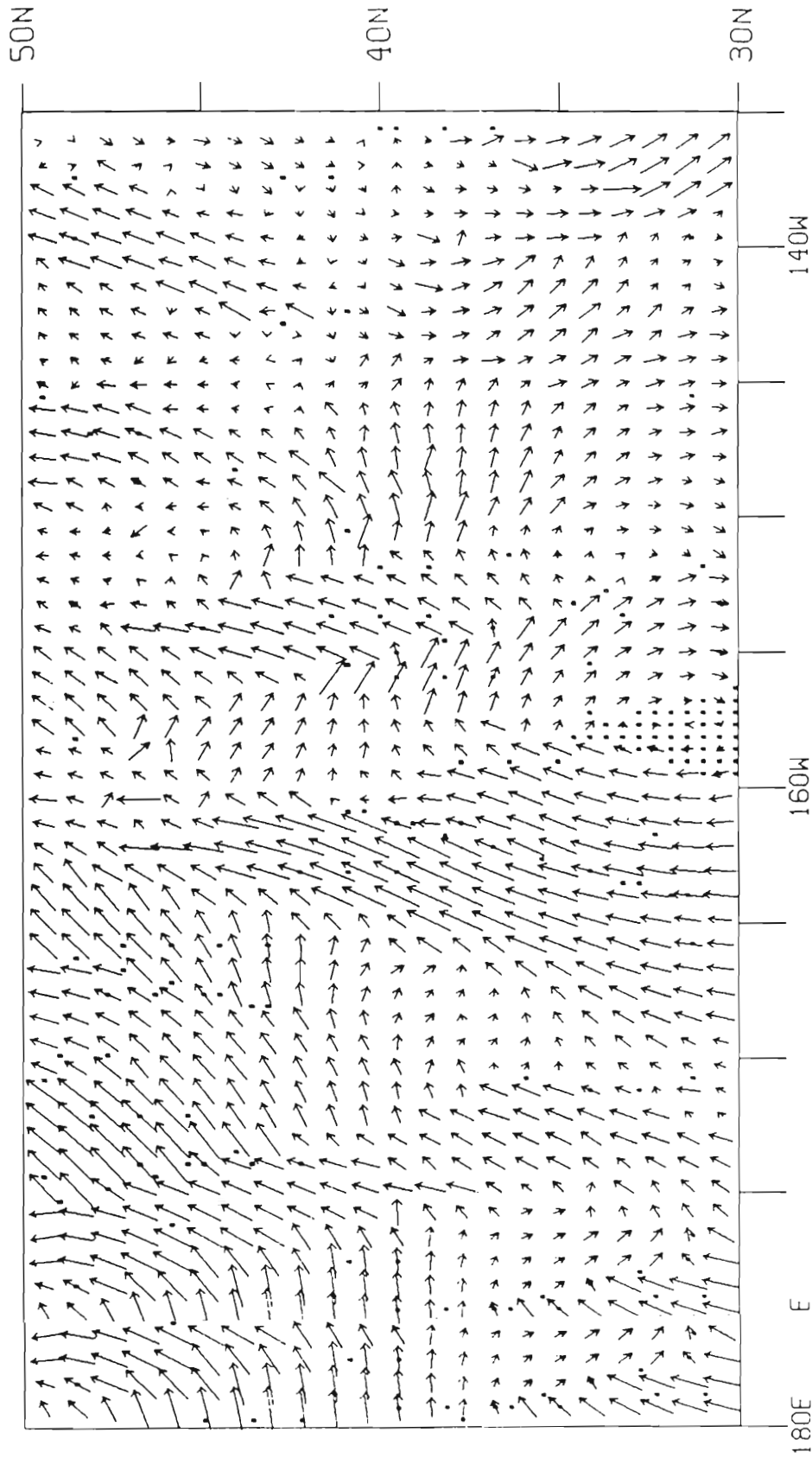


Fig. 13. Enlargement of the eastern portion of the basin in Fig. 12. Every other vector is plotted for easier analysis. Darkened circles at any location indicate interpolation was used to calculate the vector.

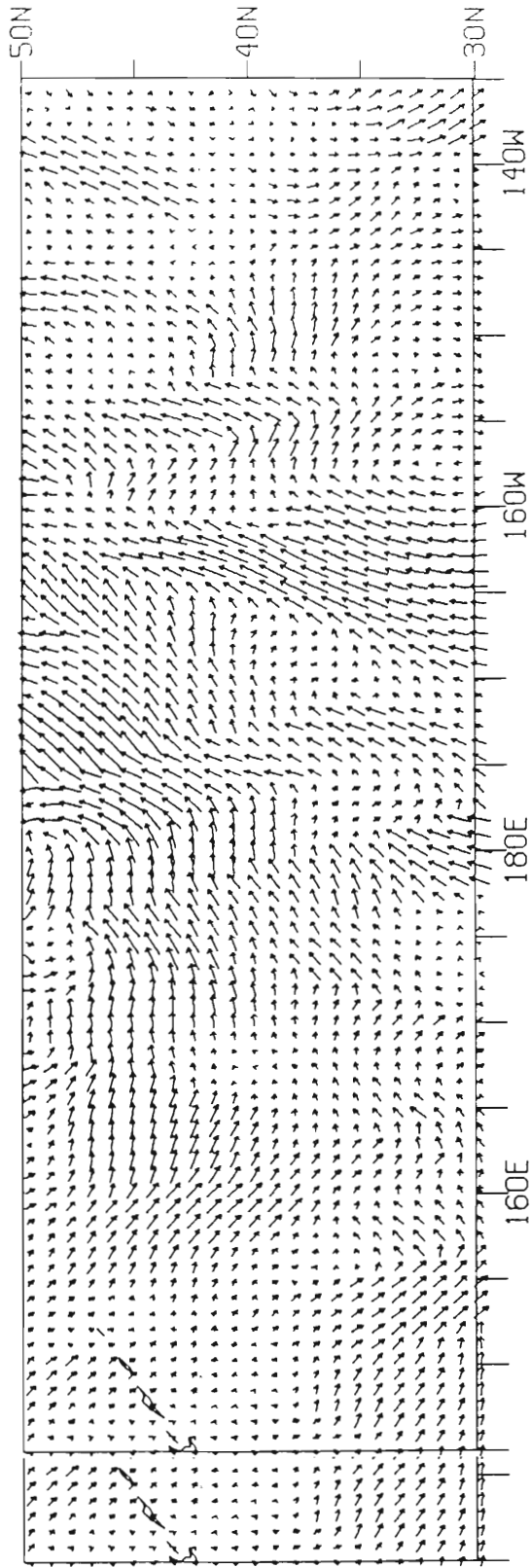


Fig. 14. The 100-km cell data from binning the 50-km cell data for the second example in the no-noise case.

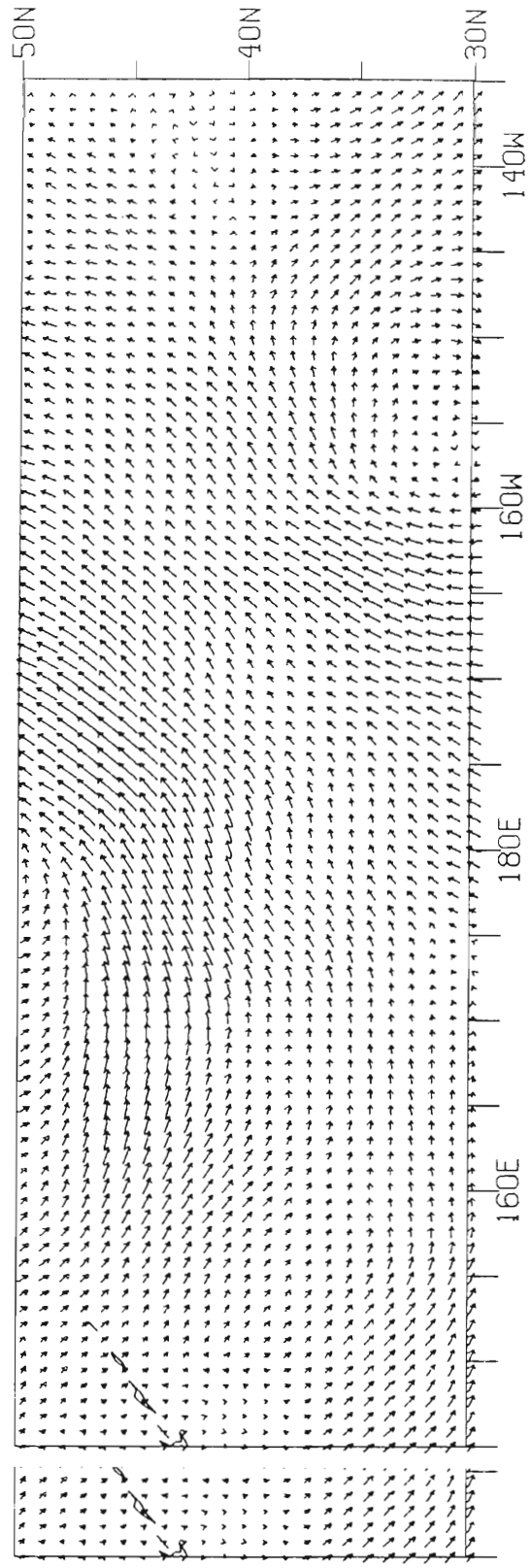


Fig. 15. The 100-km² data representing the two-day average as a result of a low-pass filter with wavenumber cutoffs of 4 in longitude and 11 in latitude for the second example in the no-noise case.

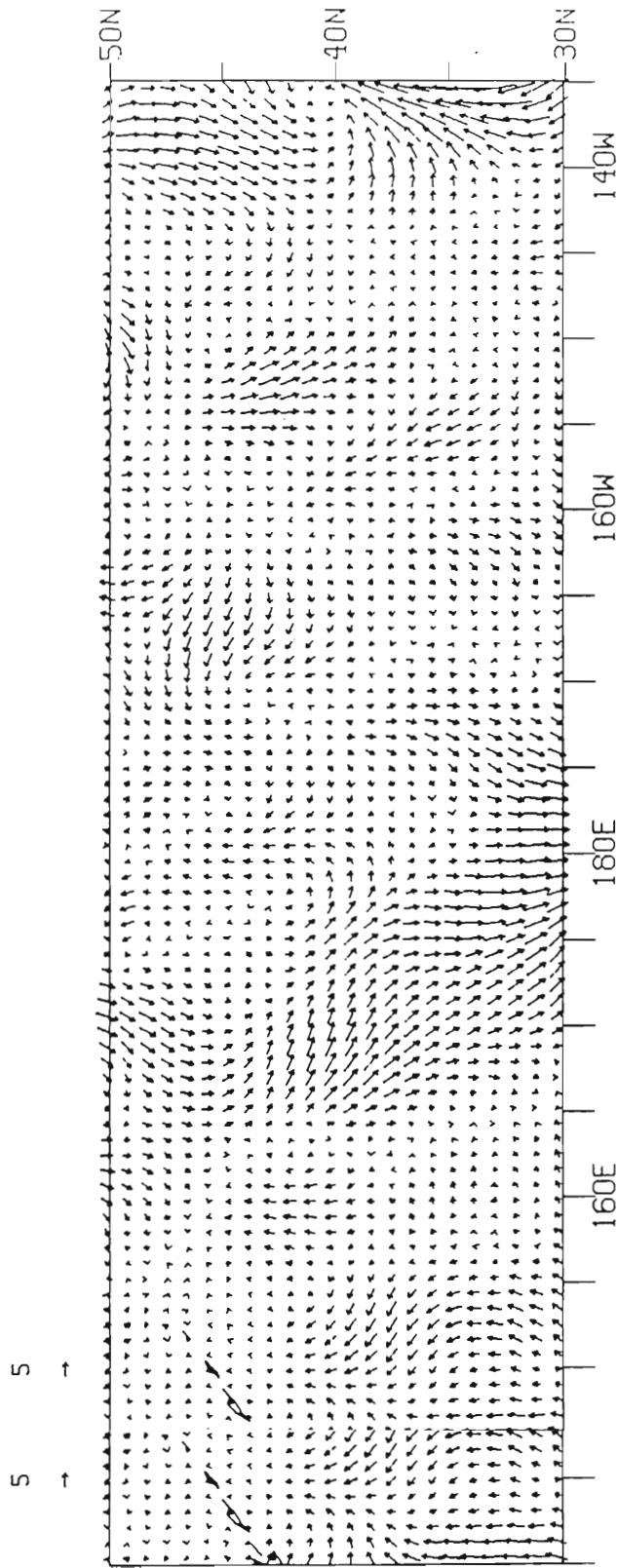


Fig. 16. Vector difference, $V_{\text{Original}} - V_{\text{Analyzed}}$, of the 100-km filtered data for the second example in the no-noise case.

between 165°E and 180°E and between 30°N and 40°N . The analysis failed to pick out the small ridge at 165°E . The analysis scheme yields winds of decreased magnitude in the southern portion of the cyclonic structure centered in the northern portion of the basin, where as these winds should have increased magnitude. Using the filter with the cutoff at such large wavenumbers also contributes to these errors. On the eastern boundary, north of 30°N and east of 145°W , there is an anticyclonic structure which was not adequately brought out by the analysis technique. Though seemingly well represented in the unfiltered data, the structure is almost completely eliminated in the filtering process. The boundary region of the basin is an area of large errors. The small scale cyclonic structure near the eastern boundary evident in the original data is not recovered in the analyzed field. The analysis did not do a very good job of extracting this structure from the data. Using a filter allowing higher wavenumbers in longitude space would probably not aid in detailing this structure since it is not evident even in the 50-km data. The high magnitude winds dominated the sampled data so that even if the scatterometer sensed a weaker structure, in this case a northerly flow into a small cyclonic structure, these smaller magnitude structures would not be realized in the analysis as they were averaged in with the larger magnitude winds. Another possible explanation is that perhaps the scatterometer never sampled the field when the structure appeared there.

explanation is that perhaps the scatterometer never sampled the field when the structure appeared there.

These two examples demonstrate how simple averaging and spectral filtering of all the sampled data can result in a data field containing most of the variability of the original data field. However, small scale structures are not fully recovered, and portions of large scale features may not be exactly correct. Overall, the analysis technique does a reasonable job of reproducing the original data although it relies only on "bits and pieces" of asynoptic data.

ANALYSIS OF DATA WITH ADDED UNCORRELATED NOISE

Inherent in any real scatterometer data are problems with noise and error. The scatterometer measurements contain noise from sources such as communication error, satellite attitude errors and errors from the empirical model to calculate the wind vectors as a function of backscatter. It would be advantageous to simulate these errors in the data set created for use in this paper. By adding noise to the optimal data set, the effect of random errors on the analysis technique can be simulated provided the noise function simulates the noise pattern in real scatterometer data.

Because of the many sources of error and quantity of data, the noise from the real scatterometer will probably be normally distributed; that is, error amplitudes will have a normally distributed probability density function. The errors will also be random which means white in a spectral representation. Noise having the above mentioned characteristics (normally distributed and random) was added to each sensed vector in the original data set of Jan. 20-21. The noise had a mean of 0 and a standard deviation of 2 ms^{-1} . This deviation magnitude approximates the expected minimum accuracy of real scatterometer data: 2 ms^{-1} , or 10% of the wind speed, whichever is greater (O'Brien, *et al.*, 1982).

speed, whichever is greater (O'Brien, *et al.*, 1982).

The 50-km gridded data are shown in Fig. 17. It is very similar to the no-noise case. The 100-km data, Fig. 18, are nearly identical to the original data. The binning process has extricated the extraneous data from the original data and produced nearly the same map. Filtering the data using the same cutoffs as used in the no-noise case resulted in the error being identical to the previous error to two significant figures. The final results are almost indistinguishable from the optimal case. Thus, noise errors of magnitude comparable to future satellite design have little impact on the analysis technique due to the binning process in calculating the data on the 100-km grid. This will not be the case when spatially coherent noise is added to the optimal data.

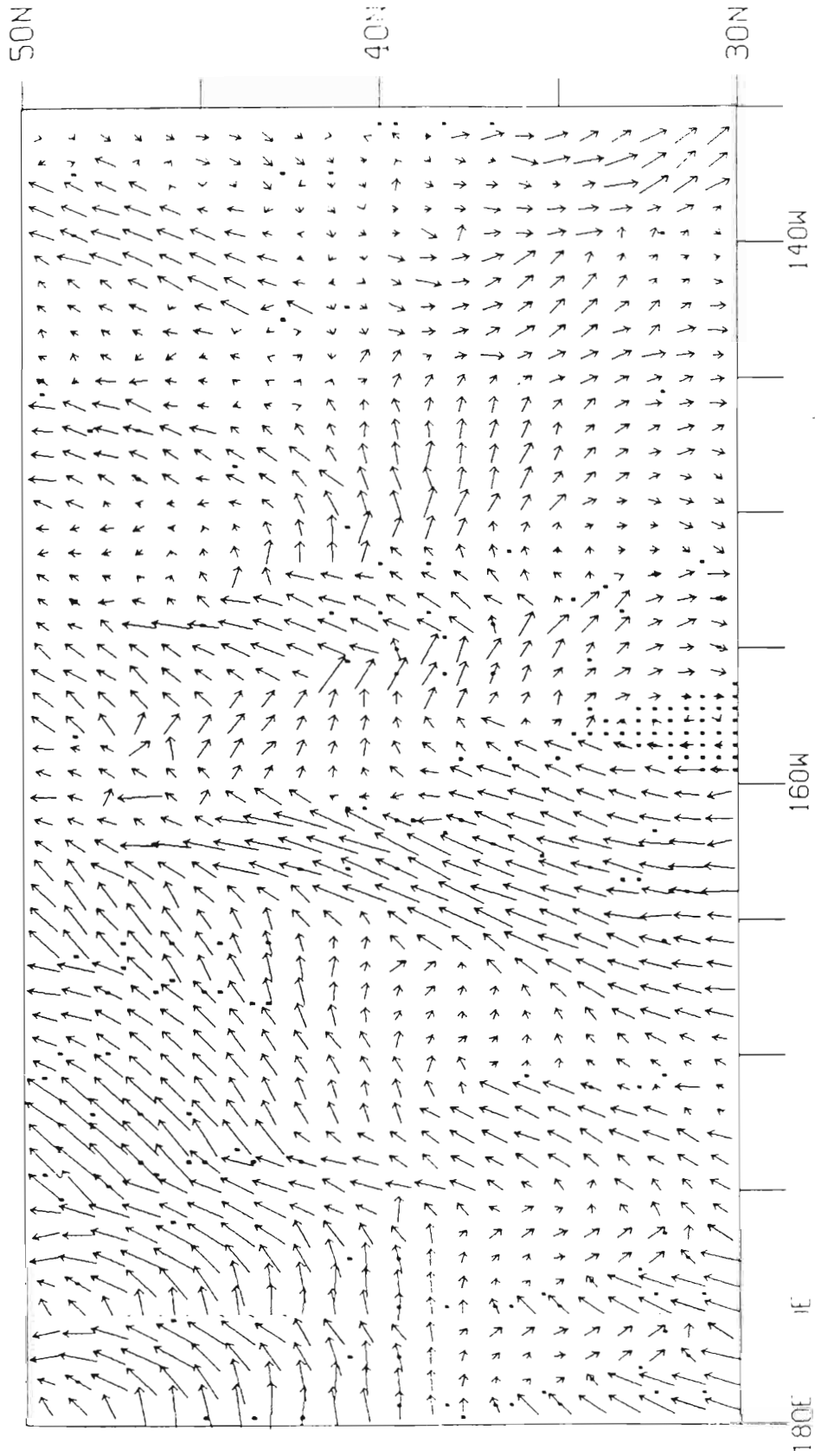


Fig. 17. Data sampled by the imaginary satellite during Jan. 20-21 in the eastern half of the basin averaged onto a 50 km grid. Uncorrelated white noise of standard deviation 2 ms⁻¹ was added to each observation. Every other vector is drawn for easier analysis. Darkened circles indicate interpolation was used to calculate the vector.

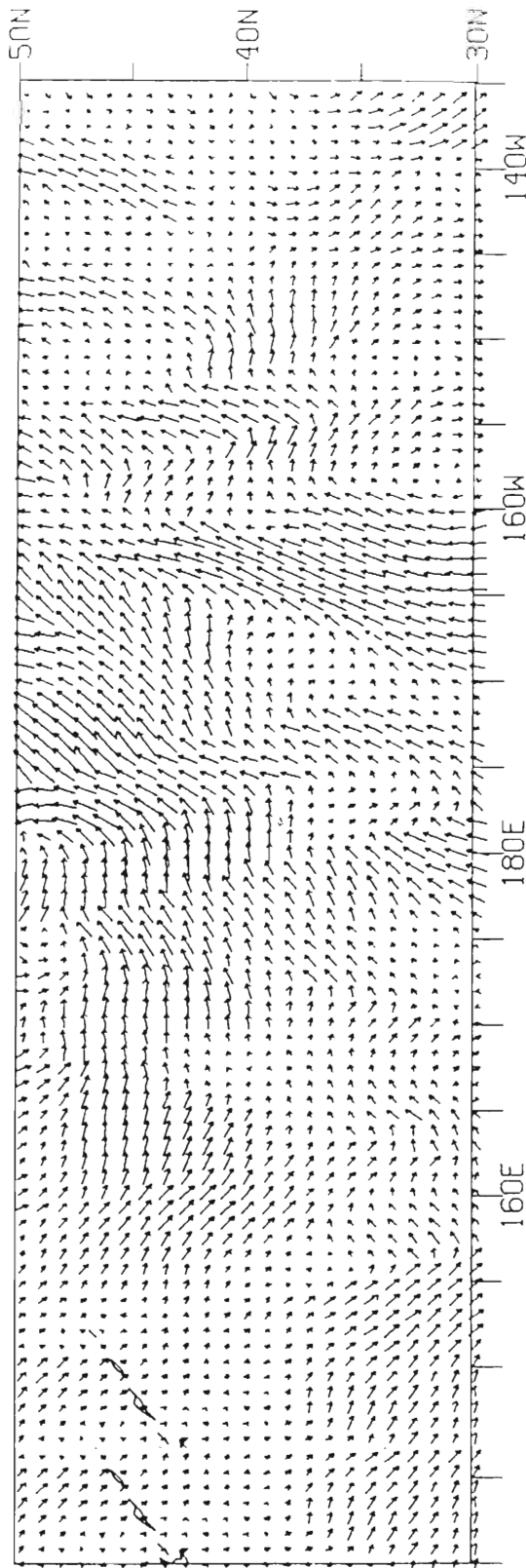


Fig. 18. The 100-km cell data from binning the 50-km cell data of Fig. 17.

ANALYSIS OF DATA WITH ADDED SPATIALLY CORRELATED NOISE

This case considers data similar to that generated in the second case. The scatterometer senses backscatter which when processed will then contain errors. In the previous case, the effects of these inherent errors due to random noise were analyzed, and it was found that for errors of the magnitude expected there were virtually no effects on the final analyzed maps. In the present case, another type of noise is added to the optimal data set of Jan. 20-21. It will be spatially correlated noise. The reason for this inclusion is straightforward.

Recall that the data for this paper was simulated using data synthesized into fields every 6 hours. The data observed by the scatterometer is generated using simple interpolation between one time and the next to find a vector at a particular location. This vector does not contain a mesoscale component. Included in the sensed vector should be some mesoscale features, though their relative amplitude is not well known as previously discussed. The spectrum of mesoscale features in surface wind fields is not well known. The added spatially correlated added noise simulates a mesoscale contribution.

The noise used in this case will be comprised of two parts.

The noise used in this case will be comprised of two parts.

Let E_{ij} be the "mesoscale" noise at location ij in a spatial grid;

$$E_{ij} = \frac{A}{4}(E_{i,j+1} + E_{i+1,j} + E_{i,j-1} + E_{i-1,j}) + \delta_{ij}$$

where δ_{ij} is a white noise generator, and E_{ij+1} , etc. are the spatially correlated noise values at the nearest four points in the grid. Of course, a more complex scheme involving any number of surrounding points could be used. The coefficient A , determines how well the noise is correlated to its 4 surrounding neighbors. The value of A can range between -1 and 1 . For A near 1 , the noise field contains large structures. If A is near 0 , structures of all scales are equally evident. Finally, if A is near -1 , all the structures will have small scales.

This correlated function for any point is a function of known and unknown quantities, therefore, successive over-relaxation is used to solve for the noise fields. The maximum error (deviation) from the desired rule is less than one percent.

Recall, the sampled data from real scatterometer data contain synoptic and mesoscale components. In the data set used in previous cases, the mesoscale component was not included. In these examples, a spatially correlated noise field was added to each sampled swath simulating the mesoscale contribution present in real scatterometer data. The noise was calculated and added as vector quantities.

Thus the added noise is correlated in each swath, but uncorrelated, swath to swath.

Thus the added noise is correlated in each swath, but uncorrelated, swath to swath.

The coefficient A , was chosen to be 0.8. This allows mostly large scale structures with some small scales included. In wavenumber space, the noise function added to each swath has a red spectrum. The spatial size of the added noise is large in comparison to the swaths, but small in comparison to the area of interest. The white noise generator regulates the variability of the added noise. How much variability should be allowed to reflect correctly the contribution of the mesoscale wind to the real scatterometer data cannot be satisfactorily addressed. In these analyses however, it is desirable to discover if the mesoscale contribution makes a difference in the results, and if so, at what level of contribution does it significantly alter the results of the analyses of the no-noise case.

The first test will begin with the January 20-21, 1979 data set. The spatially correlated noise fields were added to each swath. The noise fields were generated with $A=.8$ and δ_{ij} having a standard deviation of 2 ms^{-1} , the same variability as the uncorrelated noise added in a previous case. The mean of the added noise was 0. The map of the data binned into 50-km boxes, Fig. 19, is very similar to the map of the no-noise case. The 100-km gridded data, Fig. 20, is likewise very similar to the no-noise case. However, in these maps, some differences can be detailed. They are very subtle differences. The vectors are not as smooth as in the no-noise case. The effect is magnified in regions of low wind speed very subtle differences. The vectors are not as smooth as in the no-noise case. The effect is magnified in regions of low wind speed

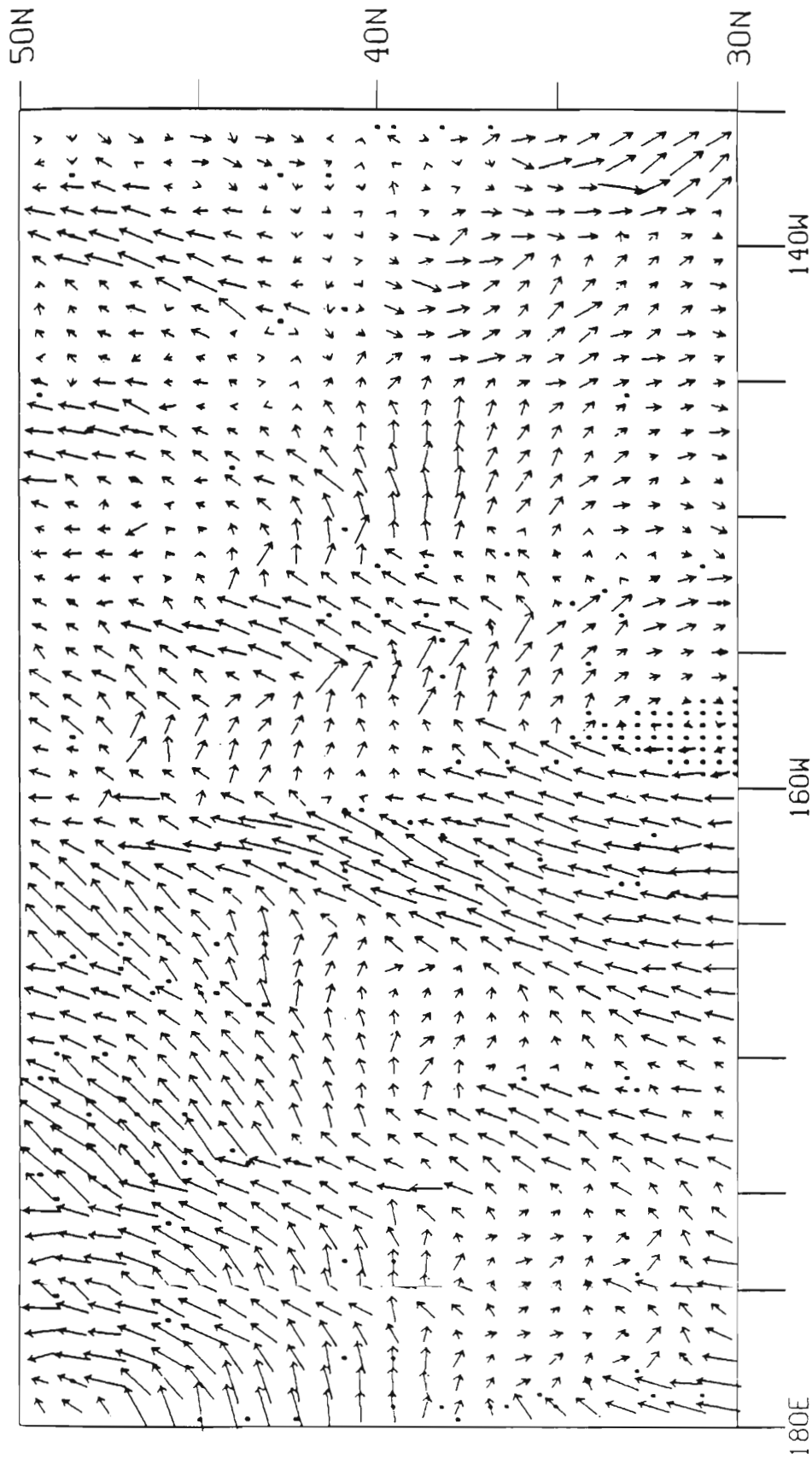


Fig. 19. Data sampled by the imaginary satellite during January 20-21 in the eastern half of the basin with spatially correlated noise with a standard deviation of 2 ms^{-1} added to each swath. Every other vector is drawn for easier analysis. Darkened circles indicate interpolation was used to calculate the vector.

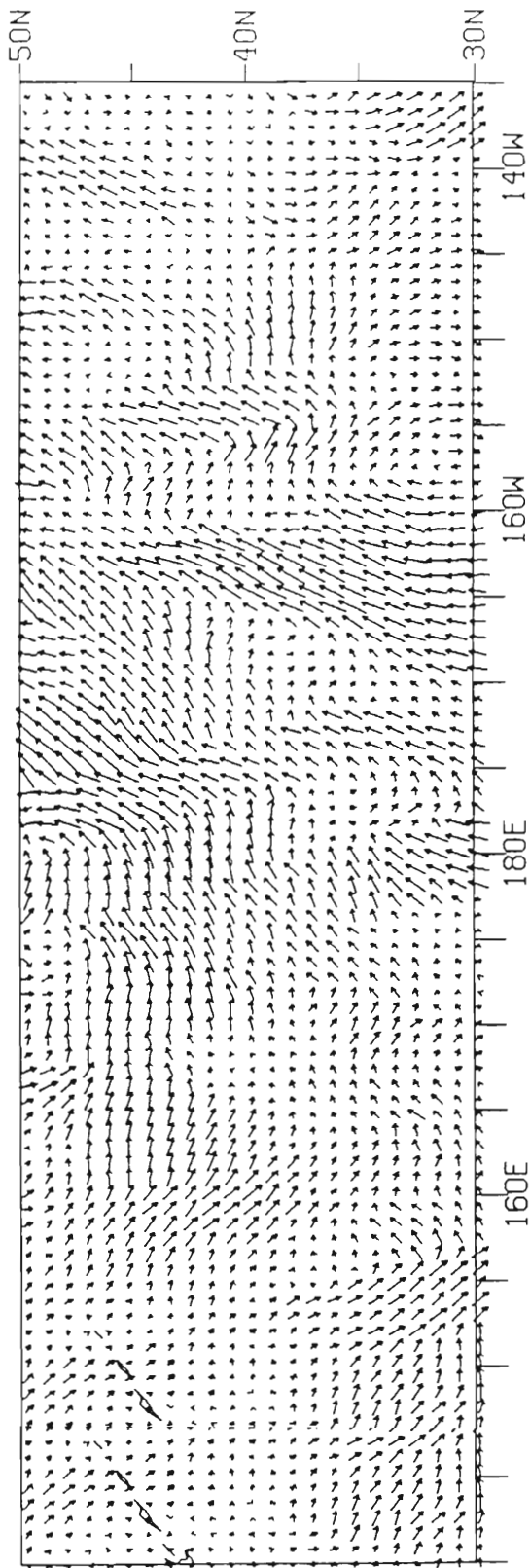


Fig. 20. The 100-km cell data from binning the 50-km cell data with spatially correlated noise of standard deviation 2 ms⁻¹ added to each swath.

where, instead of small magnitude winds in an organized structure, the winds are in seemingly random directions and not a part of an organized weather pattern.

The same filter used previously in the no-noise case yielded the best results. The cutoff values for the filter were chosen to be 4 in longitude and 11 in latitude wavenumber space, Fig. 21. The vector variance of this field is $51.5 \text{ m}^2\text{s}^{-2}$. The average magnitude of the difference vectors is 2.73 ms^{-1} , just a little larger than the no-noise case. Additionally, the vector variance of the difference field is $9.91 \text{ m}^2\text{s}^{-2}$, slightly larger than the no-noise case, but still very good. The difference map, Fig. 22, is indistinguishable from the no-noise difference map. Table 3 compares the numerical results for examples in this case.

The analysis method therefore can be said to rely almost solely on the sampling characteristics of the scatterometer. Random noise or correlated noise added to the data has little effect on the results.

The addition of correlated, structured noise results in more error than the addition of uncorrelated white noise of the same variability. This is perhaps understood when considering the effects of averaging the vector data in the first steps of these analyses. Averaging the vectors with the random noise components will tend to cancel out the effects of the added noise. When the will tend to cancel out the effects of the added noise. When the

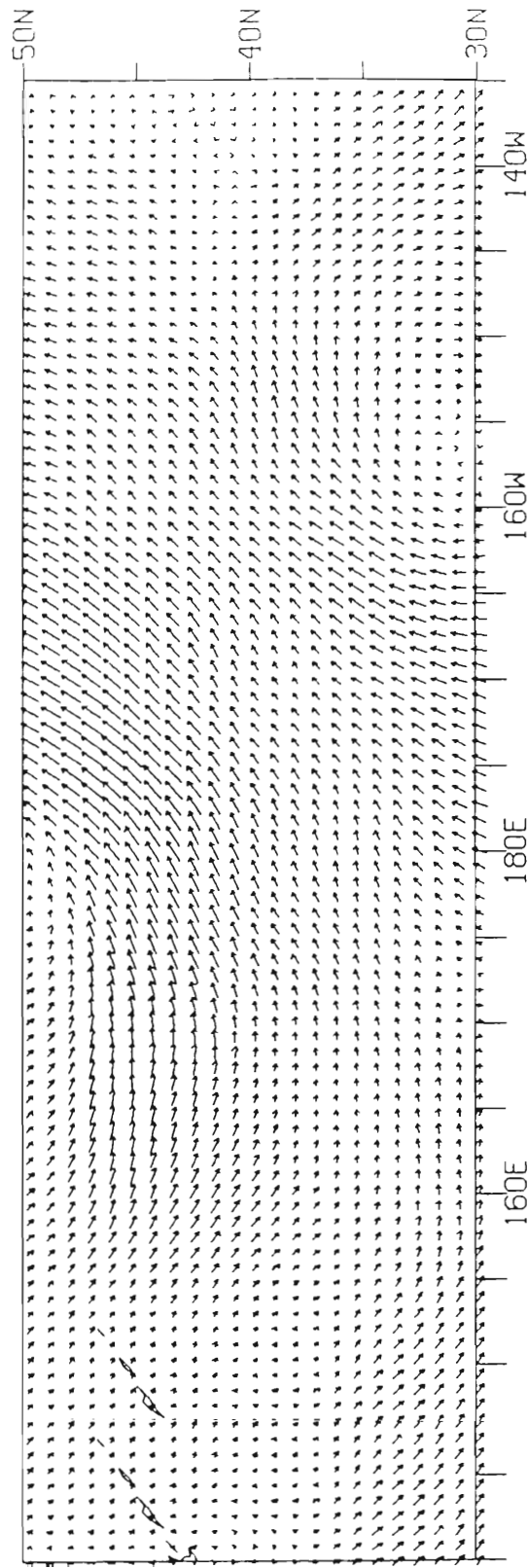


Fig. 21. The 100-km data representing the two-day average as a result of a low-pass filter with wavenumber cutoffs of 4 in longitude and 11 in latitude applied to the data in Fig. 20.

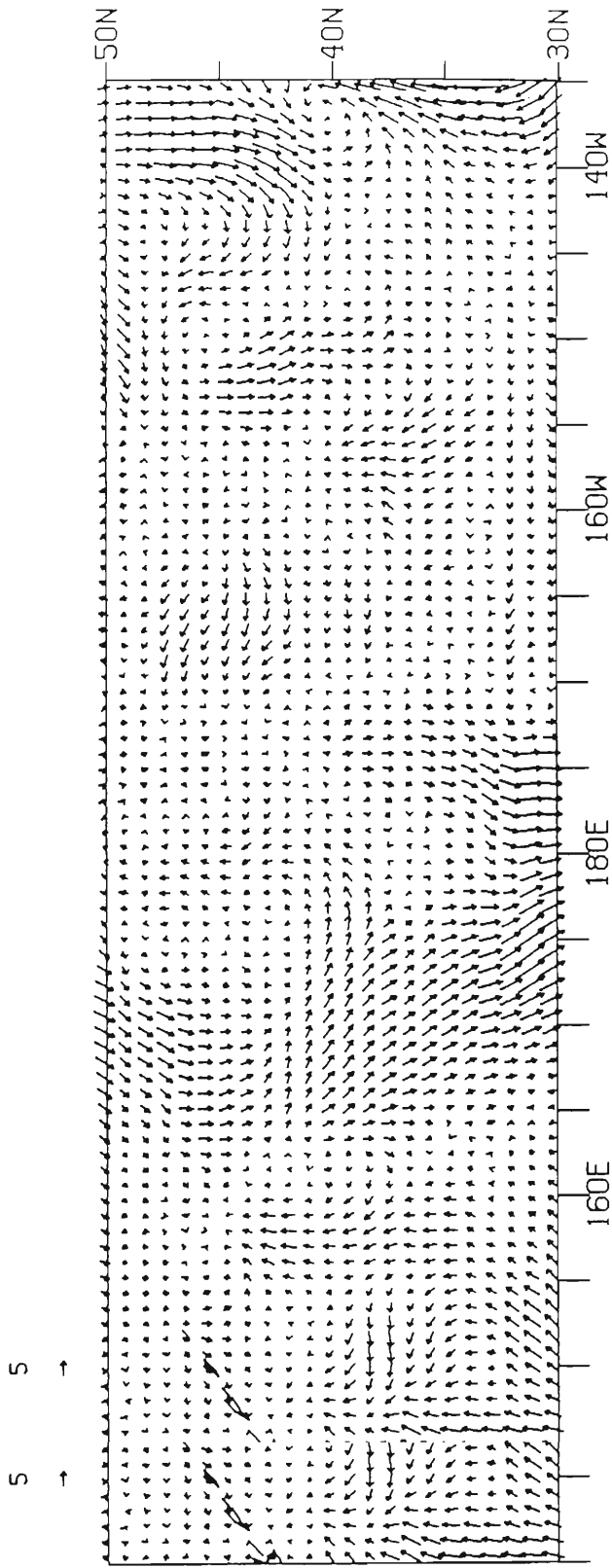


Fig. 22. Vector difference, $\vec{V}_{\text{Original}} - \vec{V}_{\text{Analyzed}}$, of the 100-km filtered data of Fig. 21.

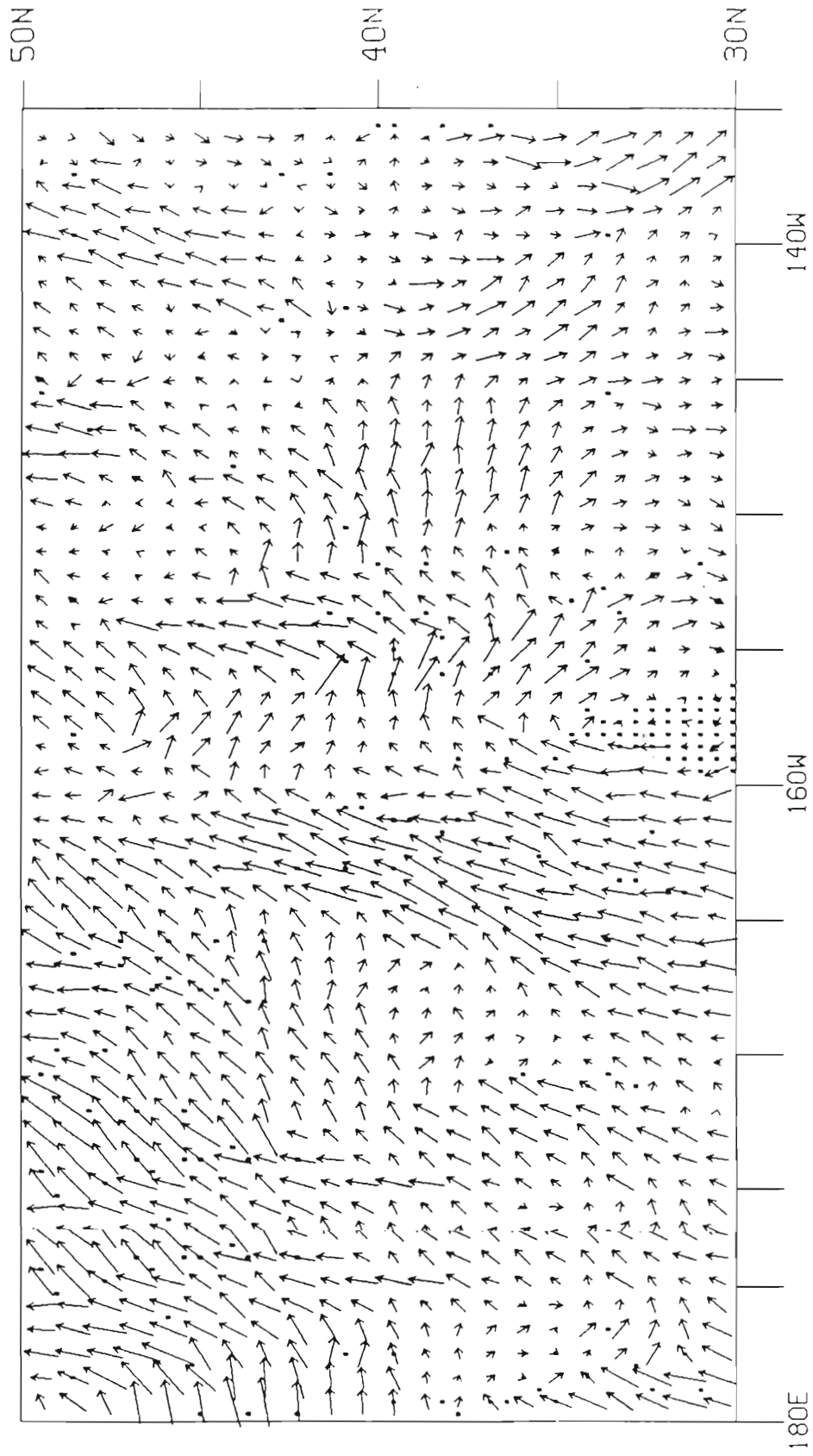
Table 3. Numerical characteristics of the method and the results for examples in the case with spatially correlated noise added to the swaths.

	Spatially correlated noise of std. dev. 2 ms ⁻¹ .	Spatially correlated noise of std. dev. 3 ms ⁻¹ .
Spatial average of temporal std. dev. ms ⁻¹ .	4.68	4.68
Vector variance of the FGGE two-day average field m ² s ⁻² .	71.79	71.79
Optimal wavenumber filter cutoff: longitude, latitude	4,11	4,8
Spatial average of difference vector magnitudes ms ⁻¹ .	2.76	2.72
Vector variance of objectively analyzed two-day average field m ² s ⁻² .	51.5	51.6
Spatial average of difference vector u components ms ⁻¹ .	1.56	1.48
Spatial average of difference vector v components ms ⁻¹ .	1.99	2.01
Vector variance of difference field m ² s ⁻² .	9.91	10.12
Vector variance of difference field m ² s ⁻² .	9.91	10.12

added noise are not random, as is the case here, averaging will carry the signature of the structured noise into the next step, and the noise will evince itself in the final resultant map.

For the final example, correlated winds with a standard deviation of 3 ms^{-1} were added to the sampled swaths. The data averaged onto the 50-km grid, Fig. 23, demonstrates how the no-noise case has been changed. The added noise has made the field quite noisy, but the gross features still remain. Adding the noise to each sampled swath increases the variability of the swaths, but averaging the sampled data into the 50-km cells decreases this variability. Only noise with very large variability will grossly change the wind field on the 100-km grid, Fig. 24. The optimal choice of cutoffs was different in this case. For the best results, cutoffs of 4 in longitude and 8 in latitude wavenumber space were used, Fig. 25. The vector variance of this field is $51.62 \text{ m}^2\text{s}^{-2}$. this is larger than the previous case. The average magnitude of the vector difference vectors is 2.72 ms^{-1} . The difference field, Fig. 26, is very similar again to previous results. The filter used dictates how the errors will be distributed. The biggest differences are in the southern region, 160°W to 140°W and the error structure from 160°E to 180° , 30°N to 40°N has changed somewhat. As can be seen, although the numerical comparisons may be similar, the vector differences are distributed differently depending on particular filter cutoffs.

vector differences are distributed differently depending on particular filter cutoffs.



Fi Fig. 23. Data sampled by the imaginary satellite during January 20-21 in the eastern half of the basin averaged onto a 50 km grid. Spatially correlated noise with a standard deviation of 3 ms^{-1} is added to each swath. Every other vector is drawn for easier analysis. Darkened circles indicate interpolation was used to calculate the vectors.

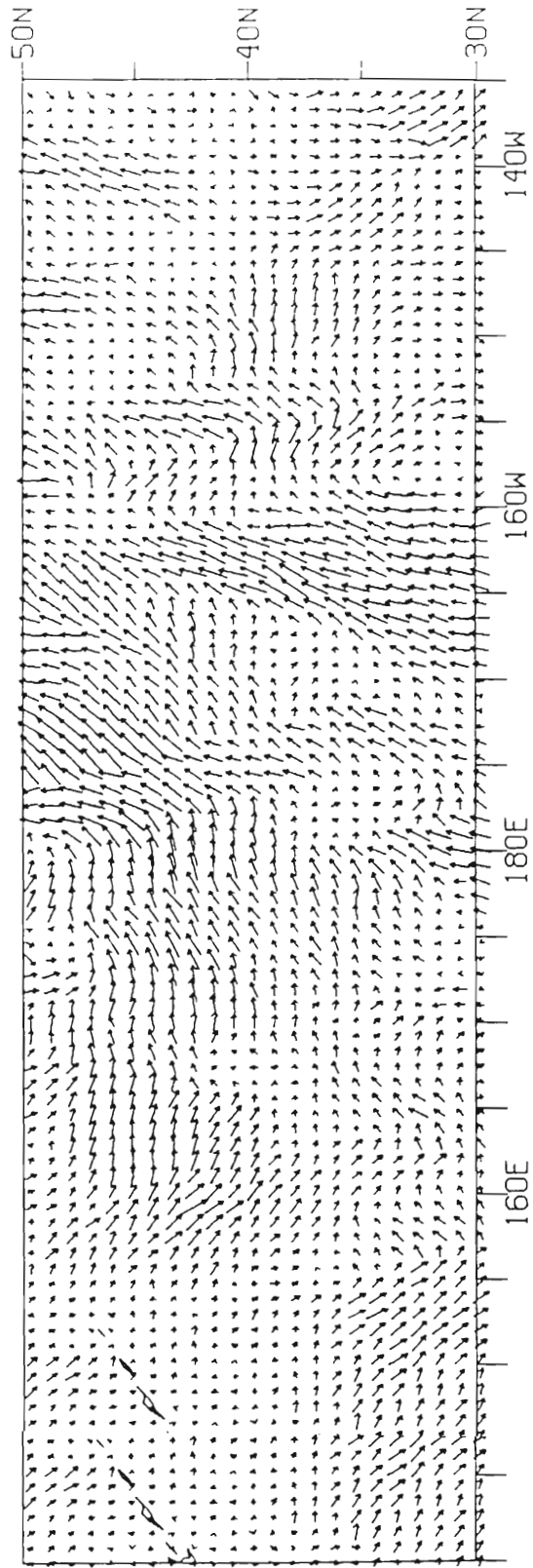


Fig. 24. The 100-km cell data from binning the 50-km cell data of Fig. 23.

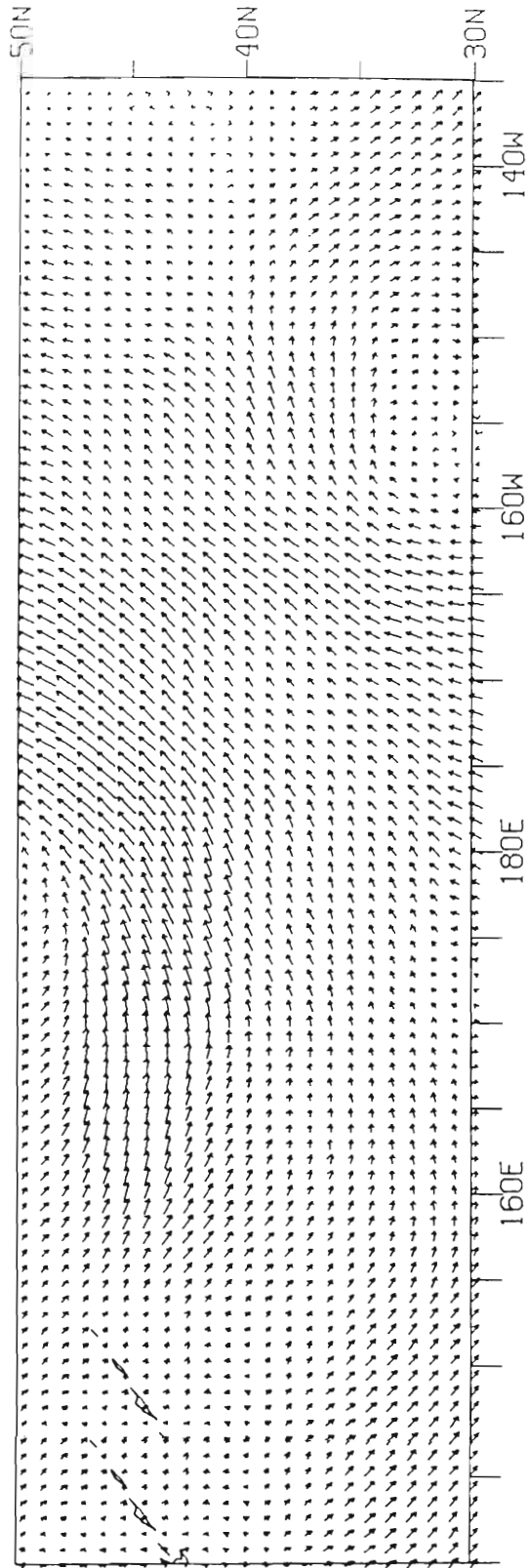


Fig. 25. The 100-km data representing the two-day average as a result of a low-pass filter with wavenumber cutoffs of 4 in longitude and 8 in latitude applied to the data in Fig. 24.

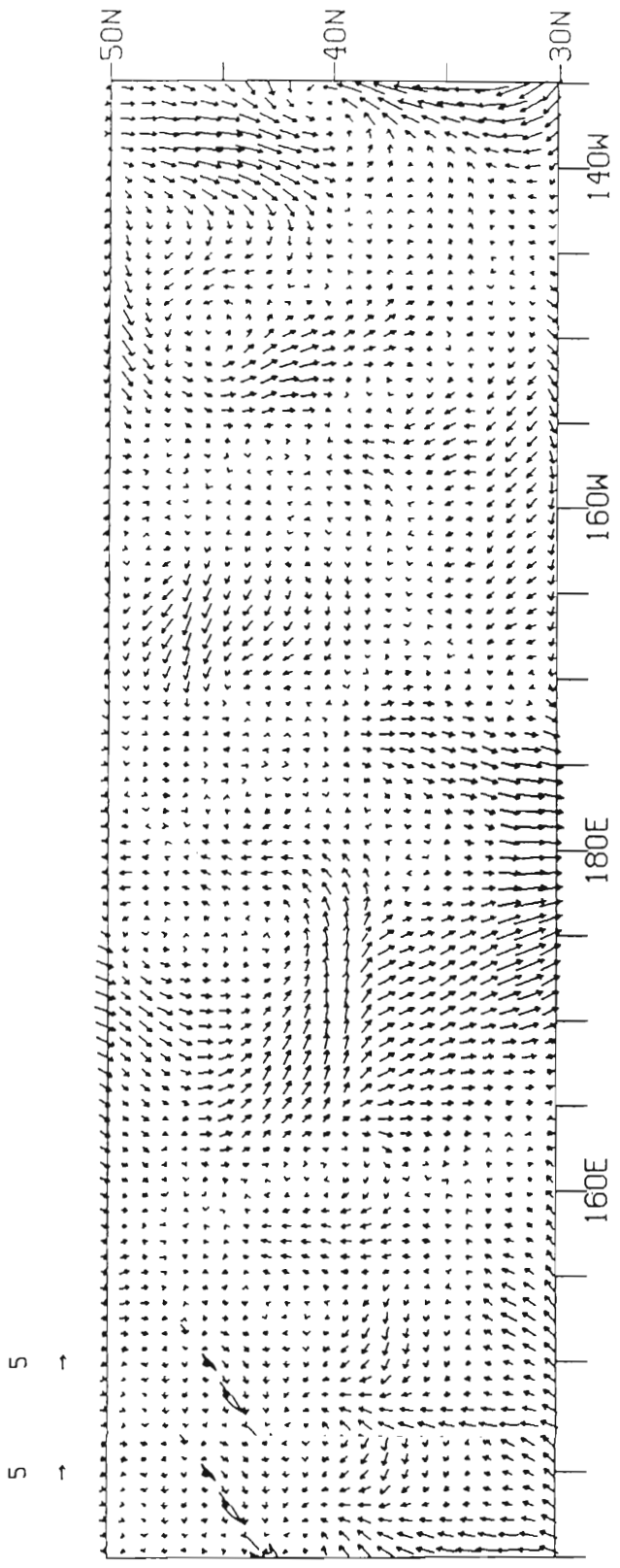


Fig. 26. Vector difference, $V_{\text{Original}} - V_{\text{Analyzed}}$, of the 100-km filtered data of Fig. 25.

Further testing of the method revealed the uncorrelated random noise and the spatially correlated noise were almost entirely filtered out using the objective analysis technique.

The spatially correlated noise added in this analysis ranged in variability from a level comparable to the expected accuracy of the scatterometer to levels nearing the variability of the true results. These additions had little effect on the analysis. The errors increased slightly, and the distribution of the errors changed as a result of tuning the wave-space filter to gain optimal results. These results again signify the dependence on the sampling characteristics of the scatterometer, rather than on instrument noise or spatially correlated noise of substantial magnitude.

DISCUSSION OF RESULTS

Results of the developed technique are very encouraging. The average magnitudes of the vector difference were never higher than about 2.75 ms^{-1} . In addition, more than the majority of the variance of the original field was contained in the resultant fields. By inspection, the method provided maps which represent well the original two-day averages. The errors are the result of the asynoptic sampling. The scatterometer simply does not function as a synoptic sampler. The largest errors occur where the vector patterns averaged onto the 50-km grid are discontinuous, particularly where the vectors shift radically in both direction and magnitude over a one-grid spacing. This, of course, is the result of swaths in close proximity. The errors are the result of using non-representative data to calculate the average. In addition, the boundary regions are a big source of error. Any structure wholly contained inside the boundary of the analysis was well represented in the analysis' representation. But, any structures with only a small portion contained in the analysis area, the cyclonic structure in the north-west quadrant of the first example no-noise case, for example, is not adequately reconstructed by the analysis method. This can be remedied by expanding the area of interest, and imposing periodic boundary conditions.

This can be remedied by expanding the area of interest, and imposing periodic boundary conditions.

The error fields still have latitudinal and longitudinal structures in them. The filter used in the method can be extensively altered to optimize the results by filtering these errors out, but since the spatial spectrum over the ocean is not well known, a carelessly constructed filter could also remove some vital components which have a physical motivation, thereby increasing the error. More than one filter may be used. For example, a band-pass filter could be used in addition to, or instead of a low-pass filter. Also, a filter in real space may provide improved results, but will reduce the data in size. An infinite number of variations in the filtering stage could be introduced to optimize the results. Since in future studies, the correct field will not be known, cutoffs cannot be varied to optimize results. I recommend wavenumber cutoffs of 4 in x and 11 in y. Structures smaller than 1500 km in longitude are filtered out.

The triangular-shaped regions in the southern portion of the basin present a problem; what criteria should be used to place data in these regions? The technique in this paper used simple, linear east-west interpolation to fill the void regions. East-west interpolation simply fills in the region with guesses based on what occurs to the east and west of each point. The vectors on either side may or may not be representative of the two-day average. Optimal interpolation or successive corrections could be used, but

Optimal interpolation or successive corrections could be used, but

using these methods does not guarantee an improvement. To demonstrate how these data-void regions affected the results, zeros were placed as observations in the data void regions for the no-noise data of January 20-21. The average magnitude of the difference vectors was 2% less than in the case when east-west interpolation was used.

Throughout the analysis cases, the magnitude of the difference vectors' meridional component, was always less than the magnitude of the zonal component, u . This is expected since most of the variability of moving frontal systems is in the meridional component. Wind structures between frontal zones are much broader and usually have steady zonal components easily picked up by the scatterometer. Frontal zones, on the other hand, are confined to small scales zonally and contain large variabilities in the meridional wind component. They are much more difficult to sample with a scatterometer, thereby resulting in more error in the meridional component representation of the wind.

SUMMARY AND CONCLUSIONS

This paper examined one problem existing with wind vector data sampled by a polar-orbiting satellite scatterometer. A technique was developed to derive synoptic fields from the asynoptically sampled fields. The FGGE level III-b data from 1000 mb in the North Pacific was used to create a simulated data set of a future scatterometer. The simulated scatterometer sampled data during two-day periods were processed using simple binning and low-pass Fourier wave-space filtering to calculate two-day averages on 100-km grids. These averages compared favorably to the original two-day averages calculated using the FGGE data.

Examples at two different times during January, 1979 were analyzed. When no errors were in the simulated scatterometer data, the average magnitude of the difference vectors on the 100-km grids were roughly 2.65 ms^{-1} : an excellent result. For the next case, uncorrelated white, normally distributed noise was added to each sampled vector to simulate random errors resulting from satellite attitude errors, communication noise errors, and errors resulting from the empirical model to calculate the wind vectors. The result was very similar to that of the first case. The effects of the added uncorrelated noise were negated in the binning process. In the last uncorrelated noise were negated in the binning process. In the last

case, spatially correlated noise simulating the effects of mesoscale structures was added to individual swaths to simulate the presence of mesoscale winds in the sampled wind fields. The added noise had increasing standard deviations of 2 and 3 ms^{-1} . All added noise had averages of 0. Each case had increased errors when compared to the no-noise case. But the error did not increase dramatically, particularly the 3 ms^{-1} example when compared to the 2 ms^{-1} example. The average magnitude of the difference vectors was about 2.75 ms^{-1} in each example, and the vector variance of the analyzed fields was about 51.5 m^2s^{-2} .

Overall results are extremely encouraging. As an operational tool, this method provides an economical, quick, and accurate representation of two-day averages on a 100-km synoptic grid. The analysis method does suffer from its relatively small area of interest, although the area of interest could be vastly expanded and perhaps lead to better results. Theoretically, this method could be expanded to cover the entire globe, but since the scatterometer can not detect wind vectors over land, this would prescribe that the globe be broken into smaller areas covering each of the world's oceanic regions.

The data set used in this paper is simulated. Using data from a real scatterometer would probably make a slight difference in the results, but once again, the analysis demonstrates the analysis' results, but once again, the analysis demonstrates the analysis'

problems are the result of the sampling pattern rather than the synoptic wind field itself. The non-sampled regions in the southern part of the basin could be filled with long-time climatological wind vectors for the time period in question. In the cases examined here, a map of average wind vectors of January could be used to fill in these regions.

The most important conclusion, of this research is the fact that the results signify the dependence on the sampling pattern rather than on instrument noise or spatially correlated noise of substantial magnitude. The technique provides very reasonable representations of the original two-day averages. Very gross features are correctly represented, but small scale variability is sometimes not well represented. The errors are also partly attributable to the particular weather patterns in the basin during the sampling time. Steady winds would provide very good results, but when moving weather systems are present and not entirely contained in the basin, this analysis technique can have problems reconstructing some details of the true data, although the overall reconstruction can be expected to be very good.

REFERENCES

- Bengtsson, L., M. Kanamitsu, P. Kallberg, and S. Uppala, 1982: FGGE 4-dimensional data assimilation at ECMWF. Bull. Am. Meteorol. Soc., 63, 29-43.
- Brown, R. A., 1983: On a satellite scatterometer as an anemometer. J. Geophys. Res., 88, 1663-1673.
- Chapman, W., and J. McGregor, 1978: The application of complex demodulation to meteorological satellite data. Quart. J. Roy. Meteor. Soc., 104, 213-223.
- Gallegos-Garcia, A., W. J. Emery, R. O. Reid, and L. Magaard, 1981: Frequency-wavenumber spectra of sea surface temperature and wind-stress curl in the Eastern North Pacific. J. Phys. Oceanogr., 11, 1059-1077.
- Hayashi, Y., 1980: A method of estimating space-time spectra from polar orbiting satellite data. J. Atmos. Sci., 37, 1385-1392.
- Jones, W. L., L. C. Schroeder, D. Boggs, E. M. Bracalente, R. A. Brown, G. Dome, W. J. Pierson, and F. J. Wentz, 1982: The SEASAT-A satellite scatterometer: The geophysical evaluation of remotely sensed wind vectors over the ocean. J. Geophys. Res., 87, 3297-3317.
- Liu, T., and W. G. Large, 1981: Determination of surface stress by SEASAT-SASS: A case study with JASIN data. J. Phys. Oceanogr., 11, 1603-1611.
- O'Brien, J. J., *et al.*, 1982: Scientific opportunities using satellite wind stress measurements over the ocean (Report of the Satellite Surface Stress Working Group), Nova University/ N.Y.I.T. Press, Ft. Lauderdale, Fla.
- Pierson, W. J., 1983: The measurement of the synoptic scale wind over the ocean. J. Geophys. Res., 88, 1683-1708.

- Salby, M. L., 1982a: Sampling theory for asynoptic satellite observations. Part I: Space-time spectra, resolution, and aliasing. J. Atmos. Sci., 39, 2577-2600.
- _____, 1982b: Sampling theory for asynoptic satellite observations. Part II: Fast Fourier synoptic mapping. J. Atmos. Sci., 11, 2601-2614.
- Pierson, W. J., and R. E. Salfi, 1982: Monte Carlo studies of ocean wind vector measurements by SCATT: objective criteria and maximum likelihood estimates for removal of aliases and effects of cell size on accuracy of vector winds, *NASA Contract Rep. 165837-1*, NASA Langley Res. Center, Hampton, Va.
- Whitney, Jr., Linwood F., 1983: International comparison of satellite winds - an update. Adv. Space Res., 2, 73-77.
- Wurtele, M. G. P. M. Woiceshyn, S. Peteherych, M. Barowski, and W. S. Applby, 1982: Wind direction alias removal studies of SEASAT scatterometer derived winds. J. Geophys. Res., 87, 3365-3377.